ARTICLES
https://doi.org/10.1038/s41591-020-0886-4

nature medicine

Check for updates

Reconstruction of the human blood–brain barrier in vitro reveals a pathogenic mechanism of APOE4 in pericytes

Joel W. Blanchard[1,2], Michael Bula[1,2], Jose Davila-Velderrain[3,4], Leyla Anne Akay[1,2], Lena Zhu[1,2], Alexander Frank[1,2], Matheus B. Victor[1,2], Julia Maeve Bonner[1,2], Hansruedi Mathys[1,2,4], Yuan-Ta Lin[1,2], Tak Ko[1], David A. Bennett[5], Hugh P. Cam[1,2], Manolis Kellis[3,4] and Li-Huei Tsai[1,2,4] ✉

In Alzheimer's disease, amyloid deposits along the brain vasculature lead to a condition known as cerebral amyloid angiopathy (CAA), which impairs blood–brain barrier (BBB) function and accelerates cognitive degeneration. Apolipoprotein (*APOE4*) is the strongest risk factor for CAA, yet the mechanisms underlying this genetic susceptibility are unknown. Here we developed an induced pluripotent stem cell-based three-dimensional model that recapitulates anatomical and physiological properties of the human BBB in vitro. Similarly to CAA, our in vitro BBB displayed significantly more amyloid accumulation in APOE4 compared to APOE3. Combinatorial experiments revealed that dysregulation of calcineurin–nuclear factor of activated T cells (NFAT) signaling and APOE in pericyte-like mural cells induces APOE4-associated CAA pathology. In the human brain, APOE and NFAT are selectively dysregulated in pericytes of APOE4 carriers, and inhibition of calcineurin–NFAT signaling reduces APOE4-associated CAA pathology in vitro and in vivo. Our study reveals the role of pericytes in APOE4-mediated CAA and highlights calcineurin–NFAT signaling as a therapeutic target in CAA and Alzheimer's disease.

The BBB is critical for proper neuronal function, protecting the brain from pathogens and tightly regulating the composition of brain fluids. Neuronal health is directly coupled to the BBB's ability to provide energy, clear waste and provide protection from peripheral pathogens[1–3]. Therefore, cerebrovascular pathologies are strong predictors of cognitive decline in the elderly[4–6]. The majority (>90%) of patients with Alzheimer's disease (AD) have amyloid deposits along their cerebral vasculature, a pathological condition known as CAA[7]. CAA impairs BBB function, rendering individuals vulnerable to cerebral ischemia, microbleeds and infections, which promote cognitive decline[8,9].

APOE4 is the strongest genetic risk factor for CAA and sporadic AD[7,10–12]. However, as the underlying molecular and cellular mechanisms are unknown, no therapeutic or lifestyle interventions exist to offset APOE4 risk for neurodegeneration. The absence of tractable human BBB models presents a major challenge for elucidating how genetics and lifestyle predispose cerebrovascular pathologies. To address these limitations and investigate the mechanisms underlying *APOE4* predisposition to CAA, we sought to reconstruct the human BBB in vitro.

Reconstruction of anatomical and physiological properties of the human blood–brain barrier in vitro. The human BBB is formed through the interactions of three cells types: brain endothelial cells (BECs), pericytes and astrocytes[13–16]. We first optimized protocols for differentiating human induced pluripotent stem cells (iPSCs) into BECs, mural cells (MCs) with pericyte-like properties, and astrocytes, with morphology and marker expression characteristic of each cell type (Fig. 1a and Extended Data Fig. 1a–i)[17–20]. Definitive identification of pericytes is challenging due to the lack of specific markers[21,22]. Therefore, to extensively characterize the identity of iPSC-derived MCs (iMCs) we performed RNA sequencing (RNA-seq), which revealed that iMCs highly express genes upregulated in pericytes relative to closely related smooth muscle cells (SMCs) and vascular fibroblasts (Extended Data Fig. 1j–m)[23,24]. Likewise, mesenchymal-associated genes (*SNAI*, *CDH1* and *AKAP1*) were not detected in iMCs but instead, robustly expressed genes associated with MCs were detected (*ACTA2*, *CD248*, *DLK1*, *PDGFRB* and *DES*) (Extended Data Fig. 1n). We next compared iMC gene expression to the global transcriptional profiles of in vivo human pericytes and SMCs generated by single-nucleus RNA-seq (snRNA-seq) of human hippocampi. Analysis of human hippocampal vascular cells identified three clusters (Extended Data Fig. 1o). Cluster 1 consists of highly expressed endothelial marker genes (*ANO2*, *ST6GALNAC3*, *ELOVL7*, *FLT1* and *ABCB1*). Cluster 2 consists of highly expressed pericyte marker genes (*LAMA2*, *GPC5*, *PDE7B*, *PDGFRB* and *DLC1*) and low levels of SMC genes (*MYH11*, *TAGLN*, *ACTA2*, *LPP* and *MYL9*) and was termed 'in vivo pericytes' (Extended Data Fig. 1o). Conversely, cluster 3 expressed low levels of pericyte marker genes, but high levels of SMC marker genes and was termed 'in vivo SMCs'. The iMCs expressed pericyte marker genes (Extended Data Fig. 1p). By unsupervised global hierarchical clustering, iMCs exhibited more similarity to human in vivo pericytes than to in vivo SMCs (Extended Data Fig. 1o). While differences between iMCs and in vivo pericytes likely exist, these data demonstrate that iMCs lack markers for fibroblasts and mesenchymal cells and exhibit a high degree of transcriptional similarity to in vivo pericytes.

[1]Picower Institute for Learning and Memory, Massachusetts Institute of Technology, Cambridge, MA, USA. [2]Department of Brain and Cognitive Sciences, Massachusetts Institute of Technology, Cambridge, MA, USA. [3]MIT Computer Science and Artificial Intelligence Laboratory, Cambridge, MA, USA. [4]Broad Institute of Harvard and MIT, Cambridge, MA, USA. [5]Rush Alzheimer's Disease Center, Rush University Medical Center, Chicago, IL, USA. ✉e-mail: lhtsai@mit.edu

BECs, iMCs and astrocytes were subsequently encapsulated in Matrigel, providing a three-dimensional (3D) extracellular matrix for self-assembly. To promote the establishment of each cell type in 3D culture, Matrigel was supplemented with 10% fetal bovine serum and growth factors (10 ng ml^{-1} platelet-derived growth factor (PDGF)-BB and 10 ng ml^{-1} vascular endothelial growth factor A (VEGFA)). After 2 weeks, BECs were assembled into large (>5 mm^2) networks of interconnected CD144$^+$ cells resembling capillaries (Fig. 1b; Extended Data Fig. 2a and Supplementary Video 1). In vivo endothelial cells secrete PDGF-BB, recruiting MCs to the perivascular space[14]. Initially, iMCs were evenly dispersed throughout the Matrigel (Extended Data Fig. 2b). However, after 2 weeks, iMCs reorganized to occupy positions proximal to BEC vessels. SM22-positive and NG2-positive cells lined large and small endothelial vessels reflective of MC in vivo coverage (Fig. 1c,d; Extended Data Fig. 2b and Supplementary Video 2). Numerous astrocytes surrounded each vessel and extended glial fibrillary acidic protein (GFAP)-positive projections into the perivascular space (Fig. 1e and Extended Data Fig. 2c). In vivo astrocytic 'end-feet' project onto capillaries, where transport molecules such as aquaporin 4 (AQP4) are localized[14,25]. In astrocyte-only cultures, AQP4 messenger RNA or protein was not detected by quantitative PCR with reverse transcription (qRT–PCR) or immunocytochemistry (Extended Data Fig. 2d,e). In contrast, our iPSC-derived BBB (iBBB) robustly expressed AQP4 mRNA and endothelial vessels were lined with S100β and GFAP-positive astrocytes expressing AQP4 (Fig. 1f; Extended Data Fig. 2d,e and Supplementary Video 3). The BBB is surrounded by a basement membrane rich in laminin-α4 (LAMA4)[26]. LAMA4 is not naturally present in Matrigel (Extended Data Fig. 2f). However, after 1 month in culture, LAMA4-immunoreactive areas surrounded endothelial vessels of the iBBB (Extended Data Fig. 2f), suggesting that iBBB cultures remodel the extracellular matrix to acquire basement membrane proteins found in in vivo BBB.

We performed transcriptional profiling by qRT–PCR of BECs cultured alone, with astrocytes or iMCs and the iBBB that included astrocytes and iMCs. Expression of BBB-associated genes *CLDN5*, *JAMA*, *PGP*, *LRP1*, *RAGE* and *GLUT1* were significantly higher in BECs from the iBBB than BECs cultured alone or co-cultured with astrocytes and iMCs, except for *CLDN5*, which was upregulated to similar levels as for iBBB when astrocytes were co-cultured with BECs (Fig. 1g)[27,28]. Numerous genes highly expressed in the BBB, including *PECAM*, *ABCG2*, *CDH5*, *CGN*, *SLC38A5*, *ABCC2*, *VWF* and *SLC7A5*, were upregulated in the iBBB model compared to BECs alone or co-cultured with astrocytes (Fig. 1h)[29]. *PLVAP*, a marker of angiogenic endothelium induced by VEGFA was upregulated in iBBB cultures[30]. *PLVAP* expression was not influenced by the presence of iMCs or astrocytes but was significantly decreased upon removal of VEGFA from culture medium (Extended Data Fig. 2g,h), suggesting that BECs in the iBBB can respond to soluble cues such as VEGFA. To minimize the effects of VEGFA and angiogenesis we subsequently cultured the iBBB in VEGFA containing medium only for the first 2 weeks of iBBB formation.

To examine physiological properties of the iBBB, we established a Transwell system consisting of a confluent monolayer of BECs on a permeable membrane with iMCs and astrocytes layered on top (Fig. 1i,j and Extended Data Fig. 2i)[16]. Trans-endothelial electrical resistance (TEER) is a sensitive and reliable indicator of permeability[31]. Peripheral endothelial cells such as human umbilical cord vascular endothelial cells (HuVECs) have relatively high permeability and thus exhibit low TEER (>150 ohm cm^2)[32]. Consistently with this, HuVECs in our Transwell configuration exhibited TEERs of approximately 100 ohm cm^2 that did not significantly change when co-cultured with astrocytes and iMCs (Fig. 1k). iPSC-derived

Fig. 1 | Reconstruction of anatomical and physiological properties of the human iBBB. a, Schematic of iBBB formation from iPSCs. **b**, iBBB stained for endothelial cell marker CD144 (red). Scale bar, 50 μm. **c**, iMCs localize to endothelial vessels after 2 weeks in culture. Scale bar, 50 μm. **d**, iMCs are labeled with NG2 (green) and BECs with CD144 (red). **e**, Astrocytes surround endothelial vessels after 2 weeks in culture. Astrocytes are labeled in green with GFAP and BECs are labeled with CD144 in red. Scale bar, 50 μm. **f**, AQP4 (green) is expressed on BEC vessels labeled with ZO-1 (red) and pan-astrocyte marker S100β is blue. Scale bar, 50 μm. Experiments in **b**–**f** were repeated at least three times each with similar results. **g**, qRT–PCR measuring expression of common BBB-associated genes. All expression is normalized to pan-endothelial marker PECAM to account for potential differences in BEC cell numbers. Mean expression and s.d. is shown of RNA collected from six independent samples for each condition. Differences were analyzed by one-way ANOVA with Bonferroni's post hoc analysis: *CLDN5*, $P < 0.0001$ for BECs (B) versus BECs + astrocytes (BA) and iBBB; *JAMA*, iBBB versus B + iMCs $P < 0.0001$, B + A, $P = 0.0009$, B only, $P < 0.0001$, B versus B + A, $P = 0.0013$, B versus B + iMCs, $P = 0.0246$; *PgP*, iBBB versus B, $P = 0.0079$, B + A, $P = 0.0001$, B + iMCs, $P = 0.0019$; *LRP1*, iBBB versus B, $P < 0.0001$, B + A, $P < 0.0001$, B + iMCs, $P < 0.0001$, B versus B + A, $P = 0.0029$; *RAGE* iBBB versus B, $P < 0.0001$, B + A, $P = 0.0357$; *GLUT1*, iBBB versus B, $P = 0.0026$. *$P > 0.05$, **$P > 0.01$, ***$P > 0.001$, ****$P > 0.0001$. **h**, qRT–PCR measuring the expression of transporters, adhesion molecules and efflux pumps and tight-junctions found in the BBB. All expression levels are normalized to BECs alone. The *y* axis is the expression level in BECs isolated from the iBBB normalized to BECs cultured alone. The *x* axis is BECs co-cultured with astrocytes normalized to BECs cultured alone. Blue circles represent means from three biological replicates and three PCR replicates. **i**, Cartoon depicting Transwell set-up for measuring iBBB permeability. **j**, Representative image of BECs (ZO-1, red), iMCs (SM22, blue) and astrocytes (S100β, green) co-cultured on a Transwell membrane. Transwell imaging experiments were repeated twice. **k**, TEER measurements from HuVECs, HuVECs plus iMCs and astrocytes, BECs only and iBBB. Circles represent single measurements from individual Transwells. Experiment consisted of six independent Transwells for each condition ($n = 6$). Dots are the means from three readings from one Transwell. Bars are means and error bars are s.d. Differences were analyzed by one-way ANOVA with Bonferroni's post hoc analysis: BECs only versus iBBB, $P = 0.0182$; BECs and iBBB versus HuVEC samples $P < 0.0001$. The TEER experiment was repeated three times with similar results. **l**, Permeability of fluorescently labeled molecules for BECs alone or iBBB. All values are reported as a percentage of each molecule's permeability across a blank Transwell membrane. Dots are the means from three permeability readings from one Transwell. Bar are means. Asterisks represent significance determined by two-sided multiple Student's *t*-test (false discovery rate (FDR) = 0.01). Cadaverine $P = 4.14 \times 10^{-8}$; 4 kDa dextran $P = 2.8 \times 10^{-5}$; 10 kDa dextran $P = 3.39 \times 10^{-6}$; transferin $P = 0.006$; 70 kDa dextran $P = 0.0006$. **m**, BBB properties of the iBBB require cooperative interaction of iMCs and astrocytes. The permeability of 4 kDa dextran was quantified in the iBBB and compared to BECs with 2× iMCs, 2× astrocytes or BECs with MEFs. Permeability was normalized to BECs alone. Each dot is the mean of three permeability readings from one Transwell with $n = 12$ Transwells per condition. Center values are mean and error bars are s.d. One-way ANOVA ($P < 0.0001$) with Bonferroni's multiple comparisons was used. **n**, *ABCG2* expression is upregulated in the iBBB. One-way ANOVA with Bonferroni's post hoc analysis ($P < 0.0001$) was used with $n = 6$ biological replicates. Each dot is the PCR mean from one biological replicate, the center value is the mean of biological replicates and error bars are s.d. **o**, Polarization of *PgP* was measured by rhodamine 123 transport for both a BECs monolayer and the iBBB from the apical (A) to basolateral (B) surface and vice versa. Inhibitor-treated samples were normalized to each respective noninhibitor-treated sample. Each dot is the mean of three permeability readings from one Transwell with $n = 6$ Transwells per condition. Center values are the mean and error bars are s.d. Asterisks represent significance determined by two-sided multiple Student's *t*-tests ($P = 0.015$) (FDR = 0.01).

BECs cultured alone had significantly higher TEERs with an average of 5,900 ohm cm^2 (Fig. 1k)[17]. However, TEERs for BECs cultured alone exhibited a high degree of variability (s.d. = ±2,150 ohm). Co-culturing BECs with iMCs and astrocytes reduced TEER variability (s.d. = ±513.9 ohm) and led to a significant increase in the average resistance (8,030 ohm cm^2) (Fig. 1k).

We next compared paracellular permeability of molecules across the iBBB. Molecules between 0.1 to 10 kDa, exhibited an approximately 50% reduction in paracellular permeability of the iBBB compared to BECs alone (Fig. 1l). Higher molecular weight molecules (70 and 80 kDa) crossed the iBBB less efficiently compared to BECs only with 70% and 90% reductions (Fig. 1l). To exclude the possibility that reduced iBBB permeability resulted from additional layers of cells, we added on top of BECs double the normal number of iMCs only, astrocytes only or a nonrelevant cell type, mouse embryonic fibroblasts (MEFs). Neither astrocytes, iMCs nor MEFs cultured alone with BECs reduced permeability, whereas the co-culture of both astrocytes and iMCs significantly reduced permeability (Fig. 1m). This demonstrates that the reduced iBBB permeability is not simply an effect of physically layering additional cells and that it requires both astrocytes and MCs.

BBB endothelial cells selectively express efflux pumps on their apical surface, an important mechanism preventing entry of many molecules into the brain[33]. We identified two common efflux pumps p-glycoprotein (*PGP*) and *ABCG2* are upregulated in the iBBB compared to BECs alone (Fig. 1g and n). To examine PGP polarization in the iBBB, we measured the efflux of rhodamine 123 in the presence and absence of the PGP-specific inhibitor reversine 121,

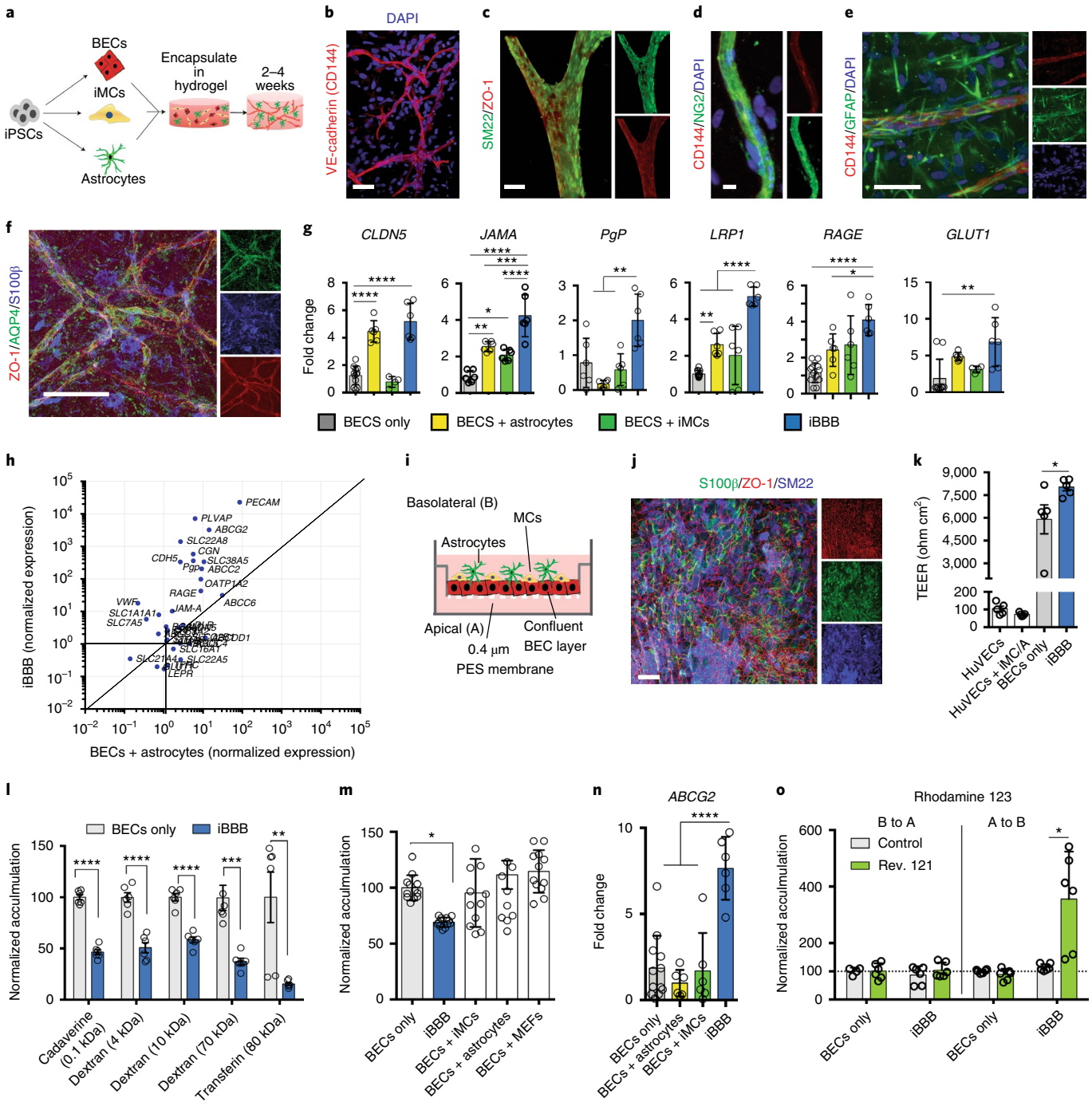

from the apical to the basolateral surface and vice versa. Inhibition of PGP dramatically increased the permeability of rhodamine 123 from the apical to the basolateral side, but not the reverse, suggesting that PGP is largely localized to the apical membrane of the iBBB (Fig. 1o)[17]. Likewise, inhibition of ABCG2 with the specific ABCG2 inhibitor KO143 also robustly increased the apical-to-basolateral transport of Hoechst 33258, an ABCG2 substrate (Extended Data Fig. 2j). This demonstrates that the iBBB has high TEER, reduced molecular permeability and polarization of efflux pumps, which are key functional properties of the BBB in vivo.

APOE4 increases Aβ accumulation in the iBBB. We next examined whether the iBBB can model AD vascular pathologies such as CAA. In vivo, the BBB is not a significant source of amyloid. Consistently with this, we detected minimal amyloid in iBBBs derived from patients with familial AD (fAD) with duplication of the *APP* gene and a separate isogenic pair with a PSEN1^{M146I} mutation and its corrected 'non-AD' control (Extended Data Fig. 3a,b). In contrast, neurons are the largest source of amyloid in the human brain[34]. Therefore, we utilized Aβ-rich conditioned medium from control and fAD neuronal cultures generated from an *APP* duplication iPSC line[35,36,37]. The iBBBs exposed to non-AD conditioned medium exhibited minimal amyloid accumulation (Fig. 2b; Fig. 2a and Extended Data Fig. 3c). In contrast, iBBBs exposed to fAD conditioned medium had marked amyloid accumulation, suggesting that the iBBB can model vascular amyloid deposition observed in vivo (Fig. 2b).

To examine whether iBBB amyloid accumulation is influenced by *APOE* genotype, we generated iBBBs from isogenic APOE3/3 and APOE4/4 iPSCs as previously reported[38]. Isogenic APOE4/4 iBBBs exposed to fAD conditioned medium consistently exhibited significantly greater 6e10-immunoreactive amyloid accumulation compared to APOE3/3 iBBBs (Fig. 2c and Supplementary Video 4). Using the reciprocal genetic editing strategy (APOE4/4-risk edited to APOE3/3-nonrisk), we again observed greater amyloid accumulation in the APOE4/4 iBBB (Fig. 2d). Unedited E3/4 heterozygous iBBBs also exhibited increased amyloid deposition compared to APOE3/3 iBBBs (Fig. 2e and Extended Data Fig. 3d), suggesting that increased amyloid deposition in the APOE4/4 iBBBs is unlikely to be the result of clonal variation or genetic editing.

We quantified iBBB amyloid accumulation with four additional methods. Using two different antibodies D54D2 (detects $A\beta_{1-37}$, $A\beta_{1-38}$, $A\beta_{1-39}$, $A\beta_{1-40}$ and $A\beta_{1-42}$), and 12F4 (detects $A\beta_{1-42}$ oligomers), we again observed that amyloid accumulation was elevated in APOE4/4 iBBBs compared to APOE3/3 (Fig. 2f,g and Extended Data Fig. 3e). Likewise, APOE4/4 iBBBs exposed to fAD conditioned medium exhibited significantly higher thioflavin T staining that binds fibril amyloid (Fig. 2g and Extended Data Fig. 3f). Similarly, exposing iBBBs to fluorescently labeled Aβ peptides (20 nM $A\beta_{1-40}$/$A\beta_{1-42}$) for 96 h led to higher levels of amyloid accumulation in APOE4/4 iBBBs, suggesting that the phenotype is not dependent upon secondary factors in conditioned medium (Extended Data Fig. 3g,h). Amyloid accumulation in the APOE4/4 iBBB corresponded with a reduction of soluble monomeric Aβ in the APOE4/4 iBBB culture medium compared to APOE3/3, further suggesting that APOE4 iBBBs accumulate more amyloid than APOE3 iBBBs (Fig. 2h).

To determine the spatial distribution of amyloid, we quantified 6e10-immunoreactive 'vascular amyloid' less than 20 µm from the center of VE-cadherin-positive vessels and 'nonvascular amyloid' greater than 20 µm from the center of a vessel (Fig. 2i). Notably, nonvascular amyloid was also increased in the parenchymal space surrounding each vessel in APOE4/4 iBBB (Fig. 2j). Nonvascular amyloid appeared in surrounding cells expressing astrocytic markers GFAP and S100β, with 36.8% of APOE4 astrocytes containing

Fig. 2 | APOE4 increases amyloid accumulation in the iBBB. a, Cartoon depicting the experimental paradigm for exposing iBBBs to exogenous Aβ. NPC, neural progenitor cell. **b**, Amyloid selectively accumulates on non-AD iBBBs exposed to medium conditioned by iPSC-derived neuronal cells from a patient with fAD with an APP duplication (APP1.1). iBBB derived from APOE3/3 iPSC line (E3/3 parental) from a healthy 75-year-old female. 6e10 antibody, green, recognizes Aβ1-16 epitope. Scale bar, 50 µm. The experiment was repeated at least three times with similar results. **c**, The APOE3/3 parental iPSC line was genetically edited to an isogenic APOE4/4 allowing the generation of genetically identical iBBBs. Isogenic APOE4/4 iBBBs accumulated more amyloid compared to the parental APOE3/3 iBBB when simultaneously exposed to APP1.1 conditioned medium for 96 h. Scale bar, 50 µm. Experiment was repeated at least three times with similar results. **d**, Representative quantification of amyloid accumulation in two isogenic iBBBs with reciprocal genetic editing strategies. Arrows indicate direction of genetic editing where the right-facing arrow indicates editing from APOE3/3 to APOE4/4 and the left-facing arrow indicates editing from APOE4/4 to APOE3/3. Total area positive for amyloid was divided by total nuclei and then normalized to the mean amyloid/nuclei from all E3/3 samples such that the mean of E3/E3 is set to 100%. Blind automated image analysis was performed with ImageJ. A two-sided Student's *t*-test was performed for data analysis ($P = 0.0114$). Twelve iBBBs were quantified for each condition. Dots represent mean amyloid across four images for each iBBB. Center values are means and error bars are s.d. **e**, APOE3/4 heterozygous iBBBs accumulate significantly more amyloid than APOE3/3 iBBBs. Quantification performed as described in d. For each condition nine iBBBs were quantified for each condition. Dots represent mean amyloid across four images for each iBBB. Center values are means and error bars are s.d. ANOVA with Bonferroni's multiple comparison test ($P < 0.0001$) was used (E3/3 versus E4/4, $P < 0.0001$; E3/3 versus sAD231, $P = 0.0055$; E3/3 versus sAD332, $P = 0.0002$; E3/3 versus H9, $P < 0.0001$). **f**, Representative images depicting that iBBBs derived from isogenic APOE3/3 and APOE4/4 individuals exhibit high levels of amyloid accumulation assay with anti-amyloid antibody D54D2. Experiments were repeated at least three times with similar results. **g**, Quantification of amyloid in isogenic iBBBs for thioflavin T ($P = 0.0258$) and two different amyloid antibodies D54D2 ($P = 0.0020$) and 12F4 ($P = 0.0054$). A two-sided Student's *t*-test was performed for data analysis. Each dot represents the mean of three images from one iBBB and six iBBBs were analyzed for this experiment. Bars center values represent mean and error bars represent s.d. Experiments were repeated twice with similar results. **h**, Quantification of soluble versus insoluble $A\beta_{1-40}$ in remaining in the iBBB culture medium 96 h after inoculation with 20 nM $A\beta_{1-40}$ ($P = 0.0319$). Two-sided Student's *t*-test was used. Each dot represents the mean of three images from one iBBB and six iBBBs were analyzed for this experiment. Bar center values represent the mean and error bars represent s.d. Experiments were repeated twice with similar results. **i**, Representative 3D IMARIS renderings depicting vascular amyloid accumulation in APOE3/3 and APOE4/4 iBBBs. The iBBBs were allowed to mature for 1 month and then were simultaneously exposed to neuronal conditioned medium from the fAD APP1.1 line. 3D surfaces of 6e10 and VE-cadherin staining were created using IMARIS software. The total area of 6e10 within 20 µm of the VE-cadherin surfaces was measured. This was normalized to the total area of the VE-cadherin surfaces. Scale bar, 10 µm. Experiments were repeated twice with similar results. **j**, Quantification of vascular (<20 µm from BEC vessel; $P = 0.0055$) and nonvascular (>20 µm from BEC vessel; $P = 0.0062$) using IMARIS software. Amyloid area was normalized to total vascular area for each image. Each dot represents the mean of three images from one iBBB and four iBBBs were analyzed for this experiment. Bar center values represent the mean and error bars represent s.d. **k**, Representative image depicting amyloid accumulation in nonvascular cells positive for the astrocyte marker S100β. Scale bar, 50 µm. Experiments were repeated twice with similar results. **l**, Quantification showing the number of astrocytes positive for amyloid for each isogenic genotype ($P = 0.0003$) using a two-sided Student's *t*-test. Each dot represents the mean of four images from one iBBB and four iBBBs were analyzed for this experiment. Bar center values represent the mean and error bars represent s.d.

amyloid compared to 16.8% of APOE3/3 astrocytes (Fig. 2k and l). In agreement, both APOE4/4 pericyte and BEC two-dimensional monocultures accumulated more fluorescently labeled Aβ than their APOE3/3 counterparts (Extended Data Fig. 3i,j).

Mural cells are required for increased Aβ deposition in the iBBB. To further determine the cellular origins of APOE4-mediated amyloid accumulation, we performed a combinatorial screen consisting of the eight possible permutations of iBBBs from APOE3/3 and APOE4/4 isogenic iPSCs. The iBBBs first matured for 1 month and were exposed to FITC-labeled Aβ for 96 h. We first categorized the iBBB permutations based on whether they exhibited low amyloid similar ($P < 0.05$) to the all APOE3/3 iBBB or high amyloid similar to the all APOE4/4 iBBB (Fig. 3a–c). Both the low and high amyloid conditions equally contained astrocytes and BECs from both APOE3/3 and APOE4/4 genotypes (Fig. 3c). However, notably, all the low amyloid conditions contained only APOE3/3 iMCs, whereas all high amyloid iBBBs contained only APOE4/4 iMCs (Fig. 3b,c). This strongly suggests that E4/4 iMCs are necessary for the increased amyloid phenotype observed in APOE4 iBBBs. Replacing only APOE4/4 iMCs with iMCs derived from a different APOE3/3 individual resulted in a significant reduction in iBBB amyloid deposition, regardless of BEC or astrocyte genotype (Fig. 3d). Substituting APOE3/3 astrocytes or BECs with APOE3/4 astrocytes or BECs did not significantly increase iBBB amyloid accumulation (Fig. 3d). However, as observed with APOE4/4 homozygous iMCs, replacing APOE3/3 iMCs with heterozygous APOE3/4 iMCs increased iBBB amyloid accumulation to a similar level as observed in the all APOE3/4 iBBB (Fig. 3d). To further confirm that APOE4 iMCs are sufficient, we deconstructed the iBBB into BECs alone, BECs with iMCs or BECs with astrocytes from each genotype. Only APOE4/4 BECs with iMCs led to a significant increase in amyloid accumulation, further suggesting that APOE4 iMCs have a casual role in iBBB amyloid accumulation (Extended Data Fig. 4a). Similarly, we exposed APOE3/3 iBBBs to medium conditioned by either APOE3/3 or APOE4/4 iMCs and then added 20 nM Aβ-FITC to all conditions. This revealed that APOE4/4 MC conditioned medium is sufficient to increase amyloid accumulation of the APOE3/3 iBBB (Fig. 3e). Treating APOE4 astrocytes with APOE4 iMC conditioned medium also significantly increased astrocytic amyloid accumulation (Extended Data Fig. 4b).

***APOE* and calcineurin signaling are upregulated in APOE4 pericytes.** RNA-seq revealed that 4,286 genes are differentially expressed genes (DEGs) ($q < 0.05$) between isogenic pericytes with 2,303 genes significantly upregulated and 1,983 genes downregulated in APOE4/4 pericytes (Fig. 4a). Gene ontology analysis suggested that the biological processes involved in protein targeting the

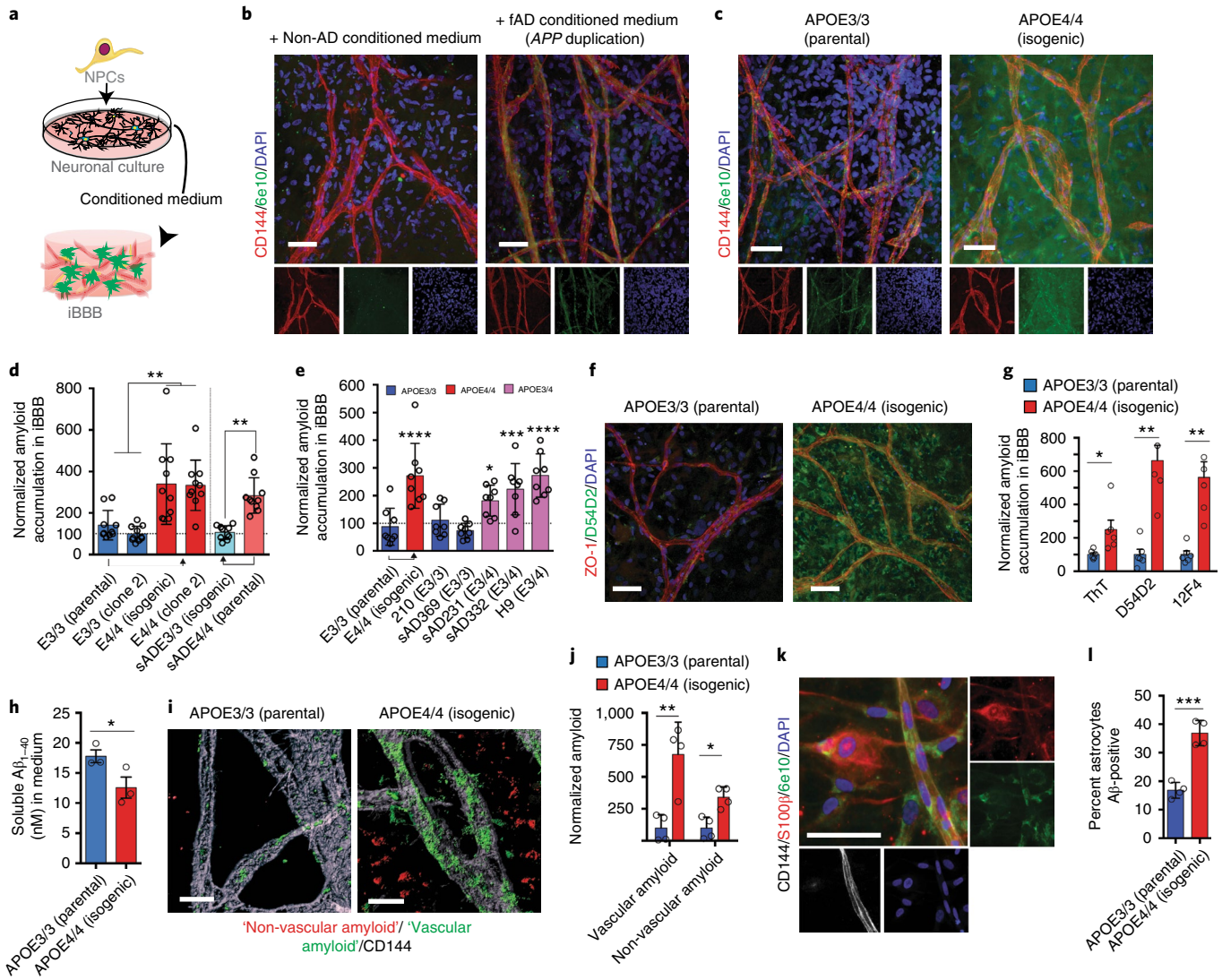

membrane and endoplasmic reticulum are upregulated in APOE4 pericytes, whereas mitosis and cell cycle progression are downregulated (Extended Data Fig. 4c). Similarly to in vivo,[39] iMCs highly express *APOE* based on relative comparison of astrocyte and pericyte *APOE* FPKM values from RNA-seq (Extended Data Fig. 5a–c). APOE4 iMCs exhibited robust upregulation of *APOE,* whereas genetically identical APOE4/4 astrocytes exhibited the reverse expression profile with reduced level of *APOE* compared to APOE3/3 (Extended Data Fig. 5d). We confirmed differential upregulation and downregulation of *APOE* in iMCs and astrocytes respectively via qRT–PCR of RNA collected from samples independently from the RNA-seq samples (Fig. 4b). APOE protein was also elevated in APOE4 iMCs (Fig. 4c,d). *APOE* gene expression was also upregulated in APOE4/4 iMCs from our reciprocal isogenic pair and multiple APOE3/4 nonedited heterozygous lines suggesting the effect is unlikely due to genetic editing or clonal variation (Fig. 4e).

Next, we examined APOE expression in human brain vasculature by further analyzing our recently published single-cell transcriptomic study of the BA10 region of human prefrontal cortex (PFC) using snRNA-seq[40]. Consistently with our in vitro studies, the PFC pericytes/endothelial cell cluster from APOE4 carriers ($n=7$ individuals) exhibited significantly higher APOE mRNA expression compared to noncarriers ($n=18$ individuals) (Extended Data Fig. 5e). APOE protein in PFC sections was also significantly higher in NG2-positive pericytes from APOE4 carriers compared to noncarriers (Extended Data Fig. 5f). We next analyzed snRNA-seq data from the hippocampus of APOE4 carriers ($n=16$ individuals) and noncarriers ($n=46$ individuals). A larger number of cells in the hippocampus dataset enabled a clear separation of endothelial cells and pericytes based on marker gene expression (Extended Data Fig. 5g). Similarly to the PFC, *APOE* expression in hippocampal pericytes from APOE4 carriers was significantly higher compared to noncarriers (Fig. 4f), whereas in endothelial cells there was no difference (Extended Data Fig. 5h). APOE4 carriers also exhibited higher APOE protein in NG2-positive pericytes compared to noncarriers by immunohistochemistry (Fig. 4g). In contrast, APOE protein in α-smooth muscle actin (SMA)-positive SMCs in the human hippocampus did not significantly differ between APOE4 carriers and noncarriers, suggesting that differential upregulation of APOE in APOE4 carriers in vivo may be restricted to pericytes (Extended Data Fig. 5i). These results suggest that in vivo APOE4 human brain pericytes express more APOE than noncarriers across multiple brain regions.

Mouse studies demonstrated that APOE is required for CAA pathologies[41] and haploinsufficiency of either APOE3 or APOE4 reduces cerebral amyloid accumulation[42]. Therefore, the increased expression of *APOE* in APOE4 iMCs in the iBBB and pericytes in vivo could promote increased amyloid accumulation. To explore this scenario, we generated isogenic APOE-truncation iPSC lines that are deficient for APOE protein (APOE knockout) using CRISPR/Cas9 editing (Extended Data Fig. 5j). APOE-deficient iBBBs exhibited low levels of amyloid, similarly to the APOE3/3 iBBBs (Fig. 4h). To test whether APOE is responsible for increased amyloid accumulation, we immunodepleted APOE from iMC conditioned medium and then exposed the APOE3 iBBBs to Aβ. Immunodepletion of APOE from the APOE4/4 iMC conditioned medium significantly reduced the accumulation of amyloid (Fig. 4i). Similarly, increasing APOE to concentrations observed in APOE4 iBBB (200 ng ml^{-1}) with recombinant APOE protein was sufficient to increase amyloid accumulation in APOE3/3 iBBB regardless of isoform (Extended Data Fig. 6a). This demonstrates that APOE protein abundance influences amyloid accumulation, suggesting that reducing APOE protein in APOE4 iMC could reduce amyloid accumulation.

Reasoning that upregulation of APOE is mediated by transcription factors, we identified transcription factors differentially expressed between isogenic APOE3/3 and APOE4/4 iMCs. In APOE4/4 iMCs, 127 transcription factors were differentially upregulated and 101 were downregulated ($q<0.05$) (Fig. 4j). Two classes of transcription factors were upregulated in APOE4/4 iMCs, NFAT (NFAT5 and NFATc1) and C/EBP, which have been reported to interact with *APOE* promoter[43]. We found the upregulation of NFAT signaling particularly interesting because it is pharmacologically tractable and reported to be dysregulated in AD brains but the consequences of elevated NFAT signaling on the cerebrovasculature are largely unknown[44].

Inactive NFAT resides in the cytoplasm, where it is phosphorylated. Upon activation, calcineurin dephosphorylates NFAT, permitting its translocation to the nucleus and interaction with gene regulatory elements[45]. APOE4 iMCs contained significantly higher cytoplasmic and nuclear NFATc1 protein as shown by immunostaining and western blotting (Fig. 4k and Extended Data Fig. 6b,c). Furthermore, genes encoding the catalytic subunits of calcineurin, *PPP3CA* and *PPP3CC* were significantly upregulated (49.8% and 26.5%, respectively) in APOE4 iMCs (Extended Data Fig. 6d). In contrast, negative regulators of calcineurin, *RCAN2* and *RCAN3*, were downregulated (−23.7% and −27.7%, respectively) in APOE4 iMCs (Extended Data Fig. 6e)[46]. *DYRK4*, (but not DYRK1-3) a kinase that phosphorylates NFAT promoting its cytoplasmic retention, was also downregulated (−38.9%) in APOE4 iMCs (Extended Data Fig. 6f). These results indicate that there are bidirectional alterations in APOE4 iMCs consistent with elevated

Fig. 3 | Mural cells are required for increased amyloid accumulation in the iBBB. a, Representative images depicting a combinatorial screen of APOE3/3 and APOE4/4 isogenic cell types reveals that APOE4 expression in iMCs is required for increased iBBB amyloid accumulation. These experiments were repeated three times. **b**, Quantification of amyloid accumulation in isogenic iBBBs for each permutation of combinatorial matrix. Each dot represents mean amyloid of four images. Six iBBBs were analyzed for each condition. Center values represent mean and error bars are s.d. Analysis was performed by one-way ANOVA with Bonferroni's multiple comparison test, where BECs/iMCs/astrocytes were 3/3/3 versus 4/4/4, $P<0.0001$; 4/4/4 versus 4/3/3, $P<0.0001$; 4/4/4 versus 4/3/4, $P=0.0004$, 4/4/4 versus 3/3/4, $P<0.0001$; 3/3/3 versus 3/4/3, $P=0.0391$; 3/3/3 versus 3/4/4, $P=0.050$; and 3/3/3 versus 4/4/3, $P=0.0023$. **c**, Segregating each isogenic permutation based on relative amyloid levels (low or high), reveals that APOE3/3 and APOE4/4 BECs and astrocytes are equally represented between the two conditions; however, iMCs are not. For the low amyloid condition only APOE3/3 iMCs are present. In contrast, for the high amyloid condition, only APOE4/4 iMCs are present. **d**, Quantification of Aβ accumulation in iBBBs derived from APO3/3 (3), H9 is APOE3/4 heterozygous and 210 is APOE3/3 homozygous. Each dot represents mean amyloid of four images. Six iBBBs were analyzed for each condition. Center values represent mean and error bars are s.d. Analysis was performed by one-way ANOVA with Bonferroni's multiple comparison test, where BECs/iMCs/astrocytes were 3/3/3 versus 4/4/4, $P<0.0001$; 4/4/4 versus 4/3/4, $P=0.0004$; 3/3/3 versus H9/H9/H9, $P=0.0018$; and 3/3/3 versus 3/H9/3, $P=0.002$. **e**, Quantification of Aβ accumulation in isogenic iBBBs and APOE3/3 iBBBs treated with iMC conditioned medium from either APOE3/3 (parental) or APOE4/4 (isogenic) iMCs. Medium was conditioned for 48 h and iBBBs were added in a 1:1 ratio of fresh medium and 20 nM Aβ-FITC for 96 h. Each dot represents mean amyloid of three images. Overall, 12 iBBBs were analyzed for each condition. Center values represent mean and error bars are s.d. Analysis was performed by two-sided Student's *t*-test, where iBBB genotype/iMC conditioned medium were 4/NA versus 3/NA, $P=0.0095$; and 3/3 versus 3/4, $P=0.001$. *$P>0.05$, **$P>0.01$, ***$P>0.001$, ****$P>0.0001$.

NFAT-mediated transcription. Indeed, genes reported to be responsive to NFAT (*ACTG2* and *VCAM1*) were upregulated in APOE4 iMCs[47,48] (Extended Data Fig. 6g).

The snRNA-seq transcriptomics analysis of the postmortem hippocampus further identified that both *NFATc1* and *NFATc2* are significantly higher in human brain pericytes from APOE4 carriers

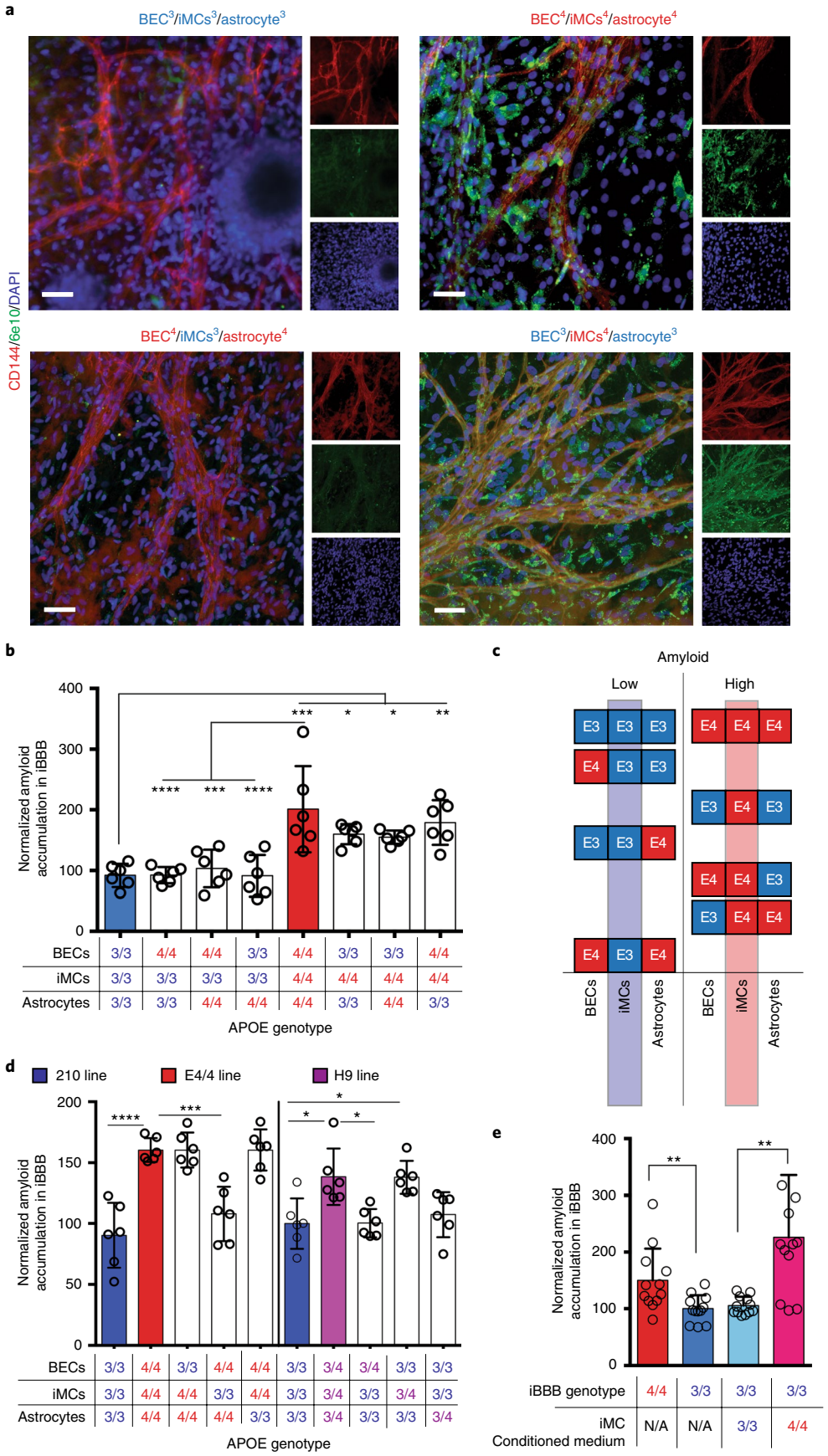

($n=16$) relative to noncarriers ($n=46$) (Fig. 4l,m). In contrast, *NFATc1* and *NFATc2* were not differentially expressed in endothelial cells (Extended Data Fig. 6h,i). In the human PFC, NFATc2 mRNA was also upregulated in human cortical pericytes/endothelial cells from APOE4 carriers compared to noncarriers via snRNA-seq (Extended Data Fig. 6j), further supporting that NFAT signaling is elevated in APOE4 pericytes in the human brain.

Inhibition of calcineurin reduces *APOE* expression and ameliorates Aβ deposition. To determine whether dysregulation of NFAT–calcineurin signaling in APOE4 pericytes contributes to upregulated *APOE* expression, we inhibited calcineurin signaling in iMCs using the well-established calcineurin inhibitors cyclosporine A (CsA) (2 µM), FK506 (5 µM) and INCA6 (5 µM) (Extended Data Fig. 7a)[49]. After 2 weeks, each of the three inhibitors significantly reduced *APOE* expression in APOE4/4 iMCs as measured by qRT–PCR (Fig. 5a). Calcineurin inhibition did not significantly reduce constitutively expressed proteins such as *PGK1*, *HPRT* and *GAPDH*, suggesting that *APOE* downregulation is not due to cellular death or global transcriptional repression (Extended Data Fig. 7b). APOE3/4 heterozygous iMCs also exhibited a significant reduction in *APOE* mRNA expression when treated with each of the three calcineurin inhibitors (Fig. 5b). Calcineurin inhibition reduced intracellular APOE protein as measured by immunofluorescence in both APOE4/4 homozygous and APOE3/4 heterozygous iMCs (Extended Data Fig. 7c,d). Likewise, CsA significantly reduced the concentration of soluble APOE protein in iMC medium measured by ELISA (Fig. 5c).

Global RNA-seq revealed that CsA treatment of iMCs reduced expression of *NFATc1* to a comparable level observed in APOE3/3 DMSO-treated iMCs (Fig. 5d). Decreased *NFATc1* correlated with reduced expression of *APOE* in APOE4 iMCs (Fig. 5e). CsA-treated APOE4/4 iMCs exhibited a transcriptional profile closer to APOE3/3 MCs (Fig. 5f). CsA treatment led to upregulation of 860 genes that exhibited similar expression levels to APOE3/3 DMSO-treated iMCs that are involved in RNA processing and peptide synthesis (Fig. 5f and Extended Data Fig. 6e). Overall, 2,783 genes exhibited moderate upregulation in response to CsA, reaching intermediate expression levels that were between APOE3/3 and APOE4/4 MCs. Gene ontology analysis categorized these genes as involved in intracellular protein transport, cellular catabolic processes and macromolecule localization (Extended Data Fig. 7e). CsA treatment also led to downregulation of 1,881 genes involved in GTPase activity and neural tube closure (Fig. 5f). Spearman's rank correlation analysis demonstrated that CsA-treated iMCs exhibited greater transcriptional similarity (0.937) to APOE3 iMCs than DMSO-treated APOE4/4 iMCs (0.889), suggesting that inhibition of calcineurin in APOE4 iMCs broadly imparts transcriptional changes that increase similarity of APOE4 MCs to APOE3 MCs.

To examine whether calcineurin inhibition can also reduce APOE4-mediated amyloid levels, we treated two isogenic pairs of iBBBs with CsA or FK506 for 2 weeks and subsequently added 20 nM of Aβ–FITC for 96 h. Both CsA and FK506 treatment led to significant reductions in amyloid accumulation in two independent APOE4/4 iBBBs compared to their isogenic APOE3/3 controls (Fig. 5g,h). In APOE3/4 heterozygous iBBBs, calcineurin inhibition also significantly reduced amyloid deposition (Fig. 5i). Similarly, conditioned medium from APOE4/4 iMCs treated with DMSO caused a significant increase in amyloid deposition in E3/3 iBBB (Fig. 5j). In contrast, medium collected from APOE4/4 iMCs treated with CsA, FK506 or INCA6 resulted in significantly reduced amyloid accumulation (Fig. 5j).

To examine whether these findings can be applied in vivo to reduce disease pathology, we first prepared cortical slice cultures

Fig. 4 | *APOE* and NFAT–calcineurin signaling are upregulated in APOE4 mural cells with pericyte-like properties in vitro and selectively in pericytes in the human brain. a, Heat map depicting DEGs between isogenic APOE3/3 and APOE4/4 iPSC-derived iMCs ($q=0.01$). RNA-seq was performed on three independent wells for each isogenic cell line. **b**, *APOE* gene expression is significantly upregulated in APOE4/4 iMCs, whereas it is downregulated in APOE4/4 astrocytes. Expression values from qRT-PCR used for RNA-seq experiment center value are means. A two-sided Student's *t*-test was used for analysis: astrocytes ($P=0.0009$) and iMCs ($P<0.0001$) ($n=9$). **c**, Immunofluorescence staining and quantification of APOE in isogenic iMCs. Scale bar, 50 µm. Dots are mean APOE fluorescence intensity from four independent images from a single well. Four wells were measured for each genotype. Unpaired two-tailed Student's *t*-test ($P=0.0005$). Center values are means. **d**, Western blot and quantification for APOE protein in APOE isogenic iMCs. Two constitutively expressed proteins in iMCs are included, SMA and GAPDH. Dots are band intensity from three independent lysates. Center values are means and error bars are s.d. Unpaired two-tailed Student's *t*-test ($P=0.0033$). **e**, qRT-PCR showing that *APOE* gene expression is also upregulated in an additional isogenic pair that was edited from E4/4 to E3/3 and three APOE3/4 heterozygous iMCs from iPSC lines derived from individuals with sporadic AD and H9 human embryonic stem cell (ESC) line. Arrows indicated the direction of genetic editing. All values are normalized to the mean expression in all APOE3/3 ($n=4$) iMCs. Center values are mean and error bars are s.d. Significance was determined by one-way ANOVA ($P<0.0001$) with Bonferroni's multiple comparison test to APOE3/3 iMCs E3/3 versus E4/4, $P=0.0002$; E3/3 versus sAD231, $P=0.0315$; E3/3 versus sAD332, $P<0.0001$; E3/3 versus H9, $P=0.0005$. **f**, Violin plots depicting *APOE* expression in pericytes isolated from postmortem hippocampus of APOE4 carriers ($n=16$ individuals) and noncarriers ($n=46$ individuals). Dashed line indicates the mean. Differential expression was measured using a two-tailed Wilcoxon rank-sum test, considering cells with detected expression of APOE. **g**, Representative images and quantification depicting the expression of APOE protein in hippocampal NG2-positive pericytes in postmortem brains from APOE4 carriers ($n=6$) and noncarriers ($n=6$). For each genotype more than 250 NG2-positive pericytes were identified. Center values are means and error bars are s.d. Two-sided unpaired Student's *t*-test was performed for analysis, $P=0.0068$. **h**, Isogenic iBBBs that are deficient for APOE by genetic knockout (KO), display similar amyloid accumulation to E3/3 iBBBs ($n=9$). Center values are mean and error bars are s.d. Significance is displayed as one-way ANOVA ($P<0.0001$) with Bonferroni's multiple comparison test, $^{**}P=0.0091$; $^{***}P=0.0006$. **i**, Immunodepleting APOE from APOE4 iMCs conditioned medium significantly reduces amyloid accumulation in the APOE3 iBBB ($n=12$). Center values are mean and error bars are s.d. One-way ANOVA ($P<0.0001$) with Bonferroni's multiple comparison test was performed, where iBBB genotype/iMC conditioned medium/immunodepletion antibody were: 3/NA/NA versus 4/NA/NA, $P=0.0051$; 3/3/NA versus 3/4/NA, $P=0.0011$; 3/3/NA versus 3/4/IgG, $P=0.0002$; 3/4/NA versus 3/4/anti-APOE, $P=0.0001$; 3/4/IgG versus 3/4/anti-APOE, $P<0.0001$. **j**, Transcription factors differentially expressed between APOE3/3 and E4/4 isogenic pairs ($q<0.05$). Blue denotes downregulated transcription factors and red dots denote upregulated transcription factors. The five transcription factors highlighted are reported to bind *APOE* gene regulatory elements. Analysis and samples are the same as described in **a**. **k**, APOE isogenic iMCs stained for NFATc1 (green) and SM22 (red). NFATc1 is present in both cytoplasm and nucleus. Dephosphorylation of NFAT by calcineurin leads to NFAT translocation to the nucleus. Quantification of NFATc1 staining per nuclei for each APOE3/3 and APOE4/4. Overall, 150 cells were analyzed for each genotype. Significance was determined by two-sided Student's *t*-test ($P<0.0001$). **l**, Violin plots depicting NFATC1 and NFATC2 expression in endothelial cells isolated from postmortem hippocampus of APOE4 carriers ($n=16$ individuals) and noncarriers ($n=46$ individuals). Differential expression was measured using a two-tailed Wilcoxon rank-sum test, $P=3\times10^{-6}$. Dashed line indicates the mean.

from APOE4KI mice, treated them with CsA or FK506 for 1 week and subsequently exposed them to Aβ–FITC for 96 h. CsA or FK506-treated cortical slices exhibited significantly less accumulation than cortical slices treated with DMSO (Extended Data Fig. 7f–h). We next isolated primary brain pericytes from APOE4KI mice[50] and subsequently treated them with DMSO, CsA or FK506 for 2 weeks. Primary brain pericytes isolated from APOE4KI mice downregulated APOE mRNA expression in response to CsA and FK506 treatment (Extended Data Fig. 7i). We next employed 6-month-old APOE4KI mice crossed to the 5XFAD mice and treated these mice with CsA (10 mg kg^{-1}) for 3 weeks via intraperitoneal injection. CsA treatment significantly reduced soluble APOE

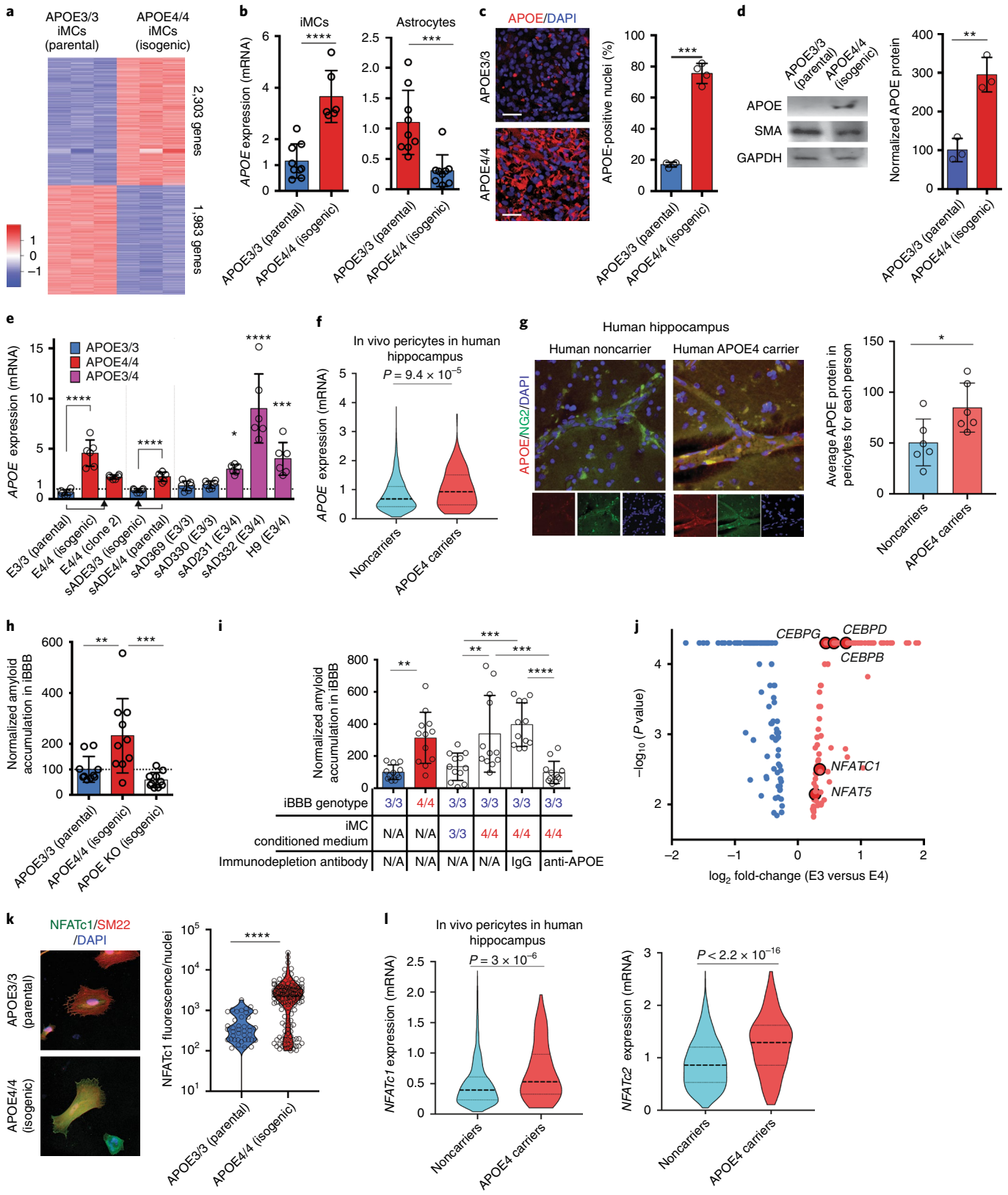

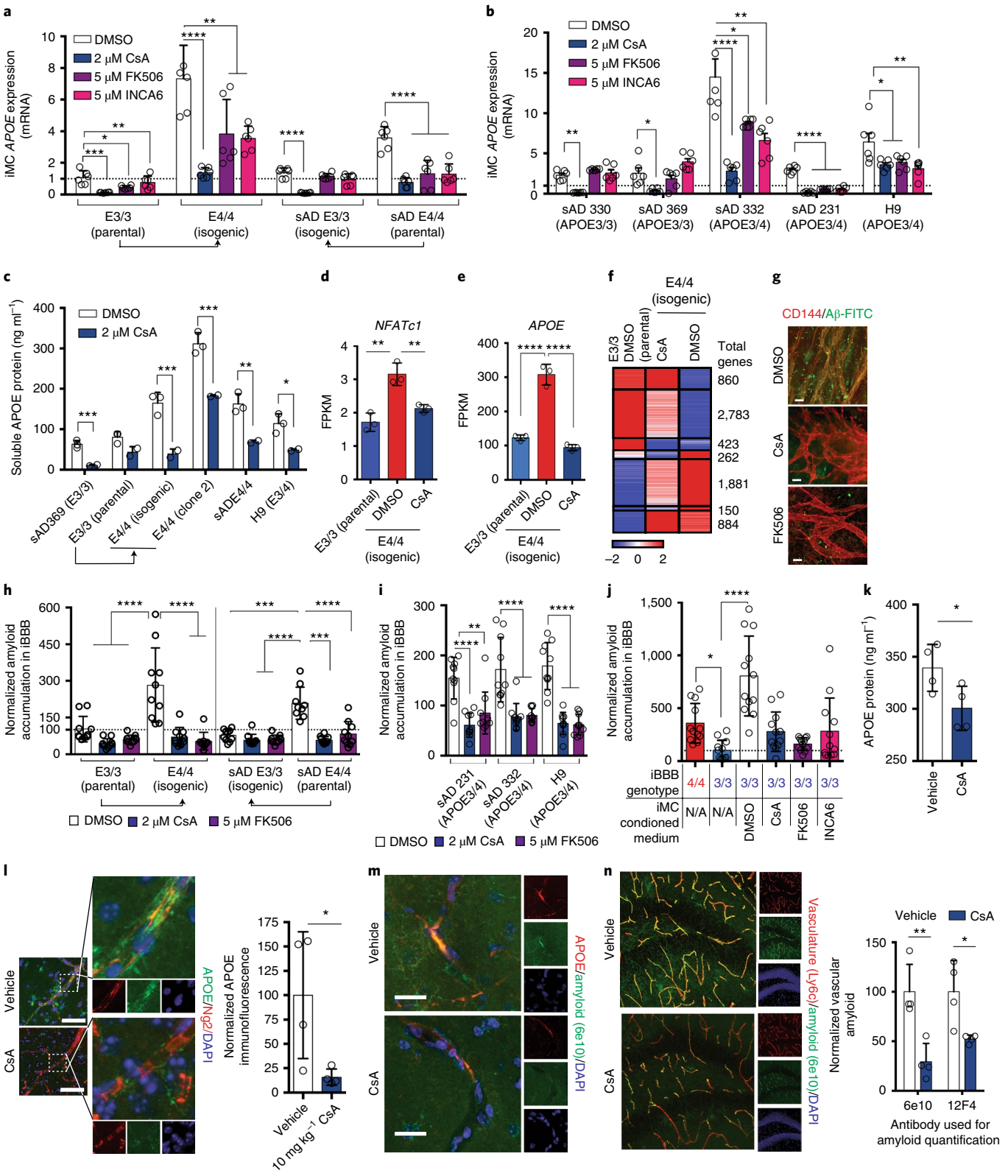

concentration in the hippocampus as measured by ELISA (Fig. 5k). APOE protein staining was also reduced surrounding NG2-positive cortical and hippocampal pericytes of CsA-treated APOE4KI × 5XFAD mice (Fig. 5l and Extended Data Fig. 7j). Co-staining for 6e10 and APOE showed that reduced APOE protein occurred simultaneously with reduced amyloid (Fig. 5m). CsA-treated mice had significantly reduced vascular amyloid when measured by two independent anti-amyloid antibodies (Fig. 5n and Extended Data Fig. 7k). This demonstrates that calcineurin–NFAT inhibition can reduce pericyte APOE levels and vascular amyloid in vivo.

Discussion

Here, we developed and validated a human in vitro model of the BBB. While the iBBB recapitulates numerous molecular and

Fig. 5 | Inhibition of calcineurin reduces *APOE* expression and ameliorates Aβ deposition. a,**b**, Expression of *APOE* in isogenic (**a**) and heterozygous (**b**) iMC after 2 weeks of treatment with DMSO, CsA, FK506 or INCA6. Significance was assessed by one-way ANOVA ($P < 0.0001$) with Bonferroni's multiple comparison. $N = 6$ RNA samples were prepared from independent wells. Center values are means and error bars are s.d. For CsA: E3/3, $P = 0.0002$; E4/4, $P = 4.52 \times 10^{-5}$; sADE3/3, $P = 1.41 \times 10^{-6}$; sADE4/4, $P = 4.717 \times 10^{-6}$. For FK506: E3/3, $P = 0.006$; E4/4, $P = 0.018$; sADE3/3, $P = 0.142$; sADE4/4, $P = 0.0005$. For INCA6: E3/3, $P = 0.226$; E4/4, $P = 0.002$; sADE3/3, $P = 0.052$; sADE4/4, $P = 0.0001$ (**a**). For CsA: sAD330, $P = 384 \times 10^{-6}$; sAD369, $P = 0.006$; sAD332, $P = 0.0004$; sAD231, $P = 2.17 \times 10^{-8}$. H9, $P = 0.025$. For CsA: sAD330, $P = 0.021$; sAD369, $P = 0.387$; sAD332, $P = 0.029$; sAD231, $P = 8.08 \times 10^{-8}$. H9, $P = 0.046$. For CsA: sAD330, $P = 0.57$; sAD369, $P = 0.095$; sAD332, $P = 0.008$; sAD231, $P = 5.6 \times 10^{-7}$. H9, $P = 0.015$ (**b**). **c**, Soluble APOE protein is significantly reduced following 2 weeks of treatment with the calcineurin inhibitor CsA. APOE concentration in iMC conditioned medium was quantified using ELISA from three separate biological replicates. Center value is mean and error bars are s.d. Significance was assessed by two-sided multiple Student's *t*-tests. Discovery was determined using the FDR method of Benjamini and Hochberg with $q = 1\%$ as follows: sAD369, $P = 0.004$; E3/3, $P = 0.06$; E4/4, $P = 0.008$; E4/4 clone 2, $P = 0.007$; sAD E4/4, $P = 0.015$; H9, $P = 0.035$. **d**,**e**, Expression of NFATc1 (**d**) and APOE (**e**) is downregulated in iMCs by CsA treatment. Bars are mean value from three biological replicates using one-way ANOVA. For NFATc1, E3/3 versus E4/4 DMSO $P = 0.0012$; E4/4 DMSO versus E4/4 CsA, $P = 0.0068$. For APOE, $P < 0.0001$) with Bonferroni's multiple comparison. Center values are mean expression from RNA prepared from three separate wells and error bars are s.d. **f**, Heat map depicting DEGs between isogenic APOE3/3 iMCs cells treated with DMSO and APOE4/4 iMCs treated with DMSO or 2 μM CsA. Genes are organized by hierarchical clustering using Spearman's rank correlation with average linkage. Boxes outline genes clustering together. The total genes for each cluster are presented on the right side of the heat map and depicted values are mean normalized counts from three independent biological replicates. **g**, Representative images of E4/4 iMCs cells treated with DMSO, CsA or FK506 for 2 weeks and then exposed to 20 nM Aβ-FITC for 96 h. Experiments were repeated at least three times (scale bar, 10 μm). **h**, Quantification of amyloid accumulation in iBBBs treated with DMSO, CsA or FK506. The iBBBs were pre-treated with chemicals for 2 weeks and then exposed to 20 nM Aβ for 96 h. Center values are mean with s.d. across ten iBBBs for each condition. Significance was determined by one-way ANOVA ($P < 0.0001$) with Bonferroni's multiple comparison: E3/3 DMSO versus E4/4 DMSO, $P < 0.0001$; E4/4 DMSO versus E4/4 CsA, $P < 0.0001$; E4/4 DMSO versus E4 FK506, $P < 0.0001$; sADE3/3 versus sADE4/4, $P = 0.0001$; sADE4/4 DMSO versus sADE3/3 CsA and FK506, $P < 0.0001$; sADE4/4 DMSO versus sADE4 CsA, $P = 0.0003$; sADE4/4 DMSO versus sADE4/4 FK506, $P < 0.0001$. **i**, Quantification of amyloid accumulation in APOE3/4 heterozygous iBBBs treated with DMSO, CsA or FK506. iBBBs were pre-treated with chemicals for 2 weeks and then exposed to 20 nM Aβ for 96 h. Center values and error bars are mean and s.d. for amyloid accumulation across ten iBBBs for each condition. Significance was determined by one-way ANOVA ($P < 0.0001$) with Bonferroni's multiple comparison. For sAD231: DMSO versus CsA, $P < 0.0001$; DMSO versus FK506, $P = 0.0023$. For sAD332: DMSO versus CsA, $P < 0.0001$; DMSO versus FK506, $P < 0.0001$. For H9: DMSO versus CsA, $P < 0.0001$; DMSO versus FK506, $P < 0.0001$. **j**, Quantification of Aβ accumulation in iBBBs treated with conditioned medium from APOE4/4 iMCs that were treated with calcineurin inhibitors for at least 1 week before medium collection. Center values and error bars are mean and s.d. for amyloid accumulation across 12 iBBBs for each condition. Significance was assessed by one-way ANOVA ($P < 0.0001$) with Bonferroni's multiple comparisons compared to E3/3 as follows: E3/3 versus E3/DMSO, $P < 0.0001$; E3/CsA, $P = 0.3413$; E3/FK506 > 0.9999; E3/INCA6, $P = 0.3112$. **k**, APOE protein concentration in the hippocampus of mice treated with either CsA or vehicle. APOE was measured by ELISA. Each dot represents mean APOE concentration from one mouse. Center value are means from four independent wells and error bars are s.d. Significance was assessed by an unpaired two-tailed Student's *t*-test ($P = 0.0456$). **l**, Representative image and quantification of immunostaining for APOE in cortical pericytes from APOE4KI × 5XFAD mice treated with CsA or vehicle. Significance was assessed by unpaired two-tailed Student's *t*-test ($P = 0.0427$). Center values are means from four mice and error bars are s.d. **m**, Representative image of concurrent reduction of vascular APOE protein and amyloid following 3-week treatment with CsA. This experiment was repeated in four mice with similar results. **n**, Representative images and quantification of vascular amyloid in the hippocampus following treatment of 6-month-old APOE4KI × 5XFAD female mice with either vehicle or CsA for 3 weeks. Amyloid was detected and quantified with two independent anti-amyloid antibodies (6e10 and 12F4). Center values are means from four mice for each condition and error bars are s.d. This experiment was repeated twice with similar results. Significance was assessed by unpaired two-tailed Student's *t*-test (6e10, $P = 0.0055$; 12F4, $P = 0.0242$). Scale bars, 25 μm. $^{*}P > 0.05$, $^{**}P > 0.01$, $^{***}P > 0.001$, $^{****}P > 0.0001$.

physiological features of the in vivo BBB there are clear differences that will benefit from future studies incorporating additional physiological aspects of the BBB and improving the fidelity of iPSC-derived vascular cells[51]. This study revealed that NFAT-mediated upregulation of APOE in human pericytes underlies the pathogenic effects of *APOE4* in CAA. We pinpoint that APOE and NFAT are dysregulated in human pericytes in the PFC and hippocampus of APOE4 carriers. We establish that chemical inhibition of calcineurin in APOE4 iMCs reduces *APOE* mRNA and protein and leads to reduced vascular amyloid accumulation. In vivo administration of calcineurin/NFAT inhibitors to APOE4 AD mice also markedly reduced *APOE* expression and vascular amyloid. Interestingly, patients chronically administered CsA or FK506 have long been observed to have significantly lower incidence of dementia compared to the general population[52]. Our results provide new insight into these observations and highlight APOE and calcineurin–NFAT-signaling as potential targets in APOE4-mediated CAA and AD.

Online content

Any methods, additional references, Nature Research reporting summaries, source data, extended data, supplementary information, acknowledgements, peer review information; details of author contributions and competing interests; and statements of data and code availability are available at https://doi.org/10.1038/s41591-020-0886-4.

Received: 30 January 2020; Accepted: 14 April 2020;
Published online: 8 June 2020

References

1. Andreone, B. J., Lacoste, B. & Gu, C. Neuronal and vascular interactions. *Annu. Rev. Neurosci.* **38**, 25–46 (2015).
2. Zlokovic, B. V. Neurovascular mechanisms of Alzheimer's neurodegeneration. *Trends Neurosci.* **28**, 202–208 (2005).
3. Iadecola, C. The neurovascular unit coming of age: a journey through neurovascular coupling in health and disease. *Neuron* **96**, 17–42 (2017).
4. Vemuri, P. et al. Vascular and amyloid pathologies are independent predictors of cognitive decline in normal elderly. *Brain* **138**, 761–771 (2015).
5. Ransohoff, R. M. How neuroinflammation contributes to neurodegeneration. *Science* **353**, 777–783 (2016).
6. Nation, D. A. et al. Blood–brain barrier breakdown is an early biomarker of human cognitive dysfunction. *Nat. Med.* **25**, 270–276 (2019).
7. Ringman, J. M. et al. Clinical predictors of severe cerebral amyloid angiopathy and influence of APOE Genotype in persons with pathologically verified Alzheimer disease. *JAMA Neurol.* **71**, 878–883 (2014).
8. Scheltens, P. & Goos, J. D. Dementia in 2011: microbleeds in dementia—singing a different ARIA. *Nat. Rev. Neurol.* **8**, 68–70 (2012).
9. Iadecola, C. The pathobiology of vascular dementia. *Neuron* **80**, 844–866 (2013).

10. Greenberg, S. M. et al. ε4 and cerebral hemorrhage associated with amyloid angiopathy. *Ann. Neurol.* **38**, 254–259 (1995).
11. Premkumar, D. R., Cohen, D. L., Hedera, P., Friedland, R. P. & Kalaria, R. N. Apolipoprotein E-epsilon4 alleles in cerebral amyloid angiopathy and cerebrovascular pathology associated with Alzheimer's disease. *Am. J. Pathol.* **148**, 2083 (1996).
12. Shinohara, M. et al. Impact of sex and APOE4 on cerebral amyloid angiopathy in Alzheimer's disease. *Acta Neuropathol.* **132**, 225–234 (2016).
13. Janzer, R. C. & Raff, M. C. Astrocytes induce blood–brain barrier properties in endothelial cells. *Nature* **325**, 253–257 (1987).
14. Armulik, A. et al. Pericytes regulate the blood–brain barrier. *Nature* **468**, 557–561 (2010).
15. Daneman, R., Zhou, L., Kebede, A. A. & Barres, B. A. Pericytes are required for blood–brain barrier integrity during embryogenesis. *Nature* **468**, 562–566 (2010).
16. Chow, B. W. & Gu, C. The molecular constituents of the blood–brain barrier. *Trends Neurosci.* **38**, 598–608 (2015).
17. Qian, T. et al. Directed differentiation of human pluripotent stem cells to blood–brain barrier endothelial cells. *Sci. Adv.* **3**, e1701679 (2017).
18. Patsch, C. et al. Generation of vascular endothelial and smooth muscle cells from human pluripotent stem cells. *Nat. Cell Biol.* **17**, 994–1003 (2015).
19. TCW, J. et al. An efficient platform for astrocyte differentiation from human induced pluripotent stem cells. *Stem Cell Rep.* **9**, 600–614 (2017).
20. Kumar, A. et al. Specification and diversification of pericytes and smooth muscle cells from mesenchymoangioblasts. *Cell Rep.* **19**, 1902–1916 (2017).
21. Armulik, A., Genové, G. & Betsholtz, C. Pericytes: developmental, physiological, and pathological perspectives, problems, and promises. *Dev. Cell* **21**, 193–215 (2011).
22. Attwell, D., Mishra, A., Hall, C. N., O'Farrell, F. M. & Dalkara, T. What is a pericyte?. *J. Cereb. Blood Flow Metab.* **36**, 451–455 (2016).
23. Vanlandewijck, M. et al. A molecular atlas of cell types and zonation in the brain vasculature. *Nature* **554**, 475–480 (2018).
24. He, L. et al. Single-cell RNA sequencing of mouse brain and lung vascular and vessel-associated cell types. *Sci. Data* **5**, 180160 (2018).
25. Bonomini, F., Francesca, B. & Rezzani, R. Aquaporin and blood–brain barrier. *Curr. Neuropharmacol.* **8**, 92–96 (2010).
26. Gautam, J., Zhang, X. & Yao, Y. The role of pericytic laminin in blood–brain barrier integrity maintenance. *Sci. Rep.* **6**, 36450 (2016).
27. O'Brown, N. M., Pfau, S. J. & Gu, C. Bridging barriers: a comparative look at the blood–brain barrier across organisms. *Genes Dev.* **32**, 466–478 (2018).
28. Urich, E., Lazic, S. E., Molnos, J., Wells, I. & Freskgård, P.-O. Transcriptional profiling of human brain endothelial cells reveals key properties crucial for predictive in vitro blood–brain barrier models. *PLoS ONE* **7**, e38149 (2012).
29. Zhao, Z., Nelson, A. R., Betsholtz, C. & Zlokovic, B. V. Establishment and dysfunction of the blood–brain barrier. *Cell* **163**, 1064–1078 (2015).
30. Strickland, L. A. et al. Plasmalemmal vesicle-associated protein (PLVAP) is expressed by tumour endothelium and is upregulated by vascular endothelial growth factor-A (VEGF). *J. Pathol.* **206**, 466–475 (2005).
31. Srinivasan, B. et al. TEER measurement techniques for in vitro barrier model systems. *J. Lab. Autom.* **20**, 107–126 (2015).
32. Deli, M. A., Ábrahám, C. S., Kataoka, Y. & Niwa, M. Permeability studies on in vitro blood–brain barrier models: physiology, pathology, and pharmacology. *Cell Mol. Neurobiol.* **25**, 59–127 (2005).
33. Seetharaman, S., Barrand, M. A., Maskell, L. & Scheper, R. J. Multidrug resistance-related transport proteins in isolated human brain microvessels and in cells cultured from these isolates. *J. Neurochem.* **70**, 1151–1159 (1998).
34. Zhang, Y. et al. An RNA-sequencing transcriptome and splicing database of glia, neurons, and vascular cells of the cerebral cortex. *J. Neurosci.* **34**, 11929–11947 (2014).
35. Israel, M. A. et al. Probing sporadic and familial Alzheimer's disease using induced pluripotent stem cells. *Nature* **482**, 216–220 (2012).
36. Chambers, S. M. et al. Combined small-molecule inhibition accelerates developmental timing and converts human pluripotent stem cells into nociceptors. *Nat. Biotechnol.* **30**, 715–720 (2012).
37. Shi, Y., Kirwan, P. & Livesey, F. J. Directed differentiation of human pluripotent stem cells to cerebral cortex neurons and neural networks. *Nat. Protoc.* **7**, 1836–1846 (2012).
38. Lin, Y. T. et al. APOE4 causes widespread molecular and cellular alterations associated with Alzheimer's disease phenotypes in human iPSC-derived brain cell types. *Neuron* **98**, 1141–1154 (2018).
39. Xu, Q. et al. Profile and regulation of apolipoprotein E (ApoE) expression in the CNS in mice with targeting of green fluorescent protein gene to the ApoE locus. *J. Neurosci.* **26**, 4985–4994 (2006).
40. Mathys, H. et al. Single-cell transcriptomic analysis of Alzheimer's disease. *Nature* **1**, 1 (2019).
41. Fryer, J. D. et al. Apolipoprotein E markedly facilitates age-dependent cerebral amyloid angiopathy and spontaneous hemorrhage in amyloid precursor protein transgenic mice. *J. Neurosci.* **23**, 7889–7896 (2003).
42. Kim, J. et al. Haploinsufficiency of human APOE reduces amyloid deposition in a mouse model of amyloid-β amyloidosis. *J. Neurosci.* **31**, 18007–18012 (2011).
43. Maloney, B., Ge, Y.-W., Alley, G. M. & Lahiri, D. K. Important differences between human and mouse APOE gene promoters: limitation of mouse APOE model in studying Alzheimer's disease. *J. Neurochem.* **103**, 1237–1257 (2007).
44. Reese, L. C. & Taglialatela, G. A role for calcineurin in Alzheimer's disease. *Curr. Neuropharmacol.* **9**, 685–692 (2011).
45. Gwack, Y. et al. A genome-wide *Drosophila* RNAi screen identifies DYRK-family kinases as regulators of NFAT. *Nature* **441**, 646–650 (2006).
46. Mulero, M. C., Aubareda, A., Schlüter, A. & Pérez-Riba, M. RCAN3, a novel calcineurin inhibitor that down-regulates NFAT-dependent cytokine gene expression. *Biochim. Biophys. Acta* **330–341**, 2007 (**1773**).
47. Lee, M. Y., Garvey, S. M., Ripley, M. L. & Wamhoff, B. R. Genome-wide microarray analyses identify the protein C receptor as a novel calcineurin/nuclear factor of activated T cells-dependent gene in vascular smooth muscle cell phenotypic modulation. *Arterioscler. Thromb. Vasc. Biol.* **31**, 2665–2675 (2011).
48. Orr, A. W., Hastings, N. E., Blackman, B. R. & Wamhoff, B. R. Complex regulation and function of the inflammatory smooth muscle cell phenotype in atherosclerosis. *J. Vasc. Res.* **47**, 168–180 (2010).
49. Kapturczak, M. H., Meier-Kriesche, H. U. & Kaplan, B. Pharmacology of calcineurin antagonists. *Transplant. Proc.* **36**, 25S–32S (2004).
50. Boroujerdi, A., Tigges, U., Welser-Alves, J. V. & Milner, R. in *Cerebral Angiogenesis* 383–392 (Humana Press, 2014).
51. Stebbins, M. J. et al. Human pluripotent stem cell-derived brain pericyte-like cells induce blood–brain barrier properties. *Sci. Adv.* **5**, eaau7375 (2019).
52. Taglialatela, G., Rastellini, C. & Cicalese, L. Reduced incidence of dementia in solid organ transplant patients treated with calcineurin inhibitors. *J. Alzheimers Dis.* **47**, 329–333 (2015).

Methods

Cell lines and differentiation. All human ESCs and human iPSCs were maintained in feeder-free conditions in mTeSR1 medium (Stem Cell Technologies) on Matrigel-coated plates (BD Biosciences). The iPSC lines were generated by the Picower Institute for Learning and Memory iPSC Facility. CRISPR/Cas9 genome editing was performed as previously described[38]. All iPSC and ESC lines used in this study are listed in Supplementary Table 1. ESCs/iPSCs were passaged at 60–80% confluence using 0.5 mM EDTA solution for 5 min and reseeding 1:6 onto Matrigel-coated plates.

BEC differentiation from iPSCs. BEC differentiation was adapted from Qian et al.[17]. Human ESCs/iPSCs were disassociated to single cells via Accutase and reseeded at 35×10^3 cm^{-2} onto Matrigel-coated plates in mTeSR1 supplemented with 10 μM Y27632 (Stem Cell Technologies). For the next 2 d, medium was replaced with mTesR1 medium daily. On the third day, the medium was changed to DeSR1 medium (DMEM/F12 with GlutaMAX (Life Technologies) supplemented with 0.1 mM β-mercaptoethanol, 1× MEM-NEAA, 1× penicillin-streptomycin and 6 μM CHIR99021 (R&D Systems)). For the following 5 d, the medium was changed to DeSR2 (DMEM/F12 with GlutaMAX (Life Technologies) supplemented with 0.1 mM β-mercaptoethanol, 1× MEM-NEAA, 1× penicillin-streptomycin and B-27 (Invitrogen)) and changed every day. After 5 d of DeSR2, the medium was changed to hECSR1 Human Endothelial SFM (Thermo Fisher Scientific) supplemented with B-27, 10 μM retinoic acid (RA) and 20 ng ml^{-1} basic fibroblast growth factor (bFGF). BECs were then split using Accutase and reseeded with hECSR1 supplemented with 10 μM Y27632. BECs were then cultured in hECSR2 medium (hECSR1 medium lacking RA + bFGF) and used within 1 week for experiments.

Pericyte differentiation protocol. Pericyte differentiation was adapted from Patsch et al.[18] and Kumar et al.[20]. The iPSCs were disassociated to single cells via Accutase and reseeded onto Matrigel-coated plates at 40,000 cells cm^{-2} in mTeSR1 medium supplemented with 10 μM Y27632. On day 1, medium was changed to N2B27 medium (1:1 DMEM/F12 with GlutaMAX and Neurobasal Medium (Life Technologies) supplemented with B-27, N-2 and penicillin-streptomycin) with 25 ng ml^{-1} BMP4 (Thermo Fisher Scientific, PHC9531) and 8 μM CHIR99021. On days 4 and 5, medium was changed to N2B27, supplemented with 10 ng ml^{-1} PDGF-BB (Peprotech, 100-14B) and 2 ng ml^{-1} Activin A (R&D Systems, 338-AC-010). Pericytes were then maintained in N2B27 medium until they were co-cultured.

NPC differentiation protocol. NPCs were differentiated using dual SMAD inhibition and bFGF supplementation as described by Chambers et al.[36].

Astrocyte differentiation protocol. Astrocytes were differentiated as described by Tcw et al.[19]. NPCs were cultured with Neurobasal NPC medium (DMEM/F12 + GlutaMAX, Neurobasal Medium, N-2 Supplement, B-27 Supplement, 5 ml of GlutaMAX, 10 ml of NEAA and 10 ml of penicillin-streptomycin) supplemented with bFGF (20 ng ml^{-1}). Astrocyte differentiation was induced using astrocyte medium (Sciencell, 1801). Astrocyte medium was changed every other day and cells were passaged at a 1:3 split at 90% confluence.

iBBB permeability studies. BECs were enzymatically dissociated by Accutase for 5 min following differentiation from iPSCs. BECs were resuspended with hECSR1 supplemented with 10 μM Y27632 onto 24-well Matrigel-coated Transwell polyester membrane cell culture inserts (0.4 μm pore size, Corning, 29442-082) at a density of 500,000–1,000,000 cells cm^{-2} to achieve a confluent monolayer. At 24 h after seeding pericytes, astrocytes or MEFs were seeded on top of the BECs at a density of 50,000 cells cm^{-2}. Permeability assays were completed when TEER values plateaued with minimum values >1,000 ohm cm^2 for two consecutive days, typically 6 d post-seeding. Then, 4 kDa, 10 kDa and 70 kDa labeled with fluorescein isothiocyanate (Sigma, 46944, FD10S, 46945), transferrin (Thermo Fisher Scientific, T-13342), Alexa Fluor 555 Cadaverine (Thermo Fisher Scientific, a30677) and BSA (Thermo Fisher Scientific, A34786) were mixed with medium and a standard curve was generated. A total of 600 μl of fresh medium was added to the bottom of the Transwell, 100 μl of dye and medium were added to the top. Permeability assays were conducted at 37 °C for 1 h. Medium from the bottom of the Transwell chamber was collected and analyzed by plate reader. For efflux transporter assays, cells were pre-incubated with 10 μM rhodamine 123 (Thermo Fisher Scientific, R302) and Hoechst dye, 5 μM reversine 121 or 5 μM KO143 (Cayman Chemical, 15215) for 1 h at 37 °C.

Three-dimensional cultures. Overall, 1×10^6 BECs ml^{-1} and 2×10^5 astrocytes ml^{-1} and 2×10^5 pericytes ml^{-1} were mixed together and encapsulated in Matrigel supplemented with 10% FBS, 10 ng ml^{-1} PDGF-BB, 10 ng ml^{-1} VEGF and 10 ng ml^{-1} bFGF. Matrigel cell solution was then seeded onto a glass-bottom culture dish. Matrigel was allowed to solidify for 40 min at 37 °C and then grown in complete astrocyte medium (SciCell) supplemented with 10 ng ml^{-1} VEGFA. After 2 weeks, VEGFA was withdrawn and iBBBs were subsequently cultured in only astrocyte medium. The 3D cultures matured for 1 month before experimentation and analysis. For imaging experiments, 3D cultures were fixed with 4% paraformaldehyde overnight at 4 °C, washed and blocked for 24 h each, then incubated with primary and secondary antibodies overnight at 4 °C each followed by a minimum of 48 h of washing.

Amyloid β accumulation. Amyloid accumulation was determined using neuronal cell conditioned medium and 20 nM recombinant-labeled Hilyte fluor 488 $A\beta_{1-40}$ (Anaspec, AS-60491-01) and $A\beta_{1-42}$ (Anaspec, AS-60479-01) resuspended in PBS. Aβ accumulation for each cell line and experimental permutation was determined from two-dimensional cultures containing all three cells types containing the same ratio of cells as the 3D experiments. The total area positive for Aβ was divided by the total number of nuclei and normalized to experimental controls. At least four images for each biological replicate were analyzed and for each condition at least three biological replicates were employed. Two-dimensional quantifications were corroborated by 3D imaging and analysis.

Immunofluorescence staining and APOE immunodepletion. Cells were washed with PBS and fixed for 15 min with 4% paraformaldehyde (Electron Microscopy Sciences, 15714-S). Samples were then washed with PBS three times for 5 min followed by a permeabilization in PBST for 30 min. Cells were blocked in PBST (0.1% Triton X-100) containing 5% normal donkey serum (Millipore, S30) and 0.05% sodium azide. Primary antibody staining was performed overnight at 4 °C. Primary and secondary antibodies are listed in Supplementary Table 1. Cells were washed three times for 5 min with PBST and incubated for 1 h at room temperature with secondary antibody. For immunodepleting experiments, APOE was immunodepleted from pericyte conditioned medium by incubating conditioned medium with 5 μg of anti-APOE or nonspecific IgG control antibodies overnight at 4 °C. Antibodies were then removed with magnetic protein A/G beads.

Western blot and ELISA lysis preparation. Cells were washed with PBS and dissociated using Accutase. Cells were then counted using a hemocytometer with Trypan blue and normalized to total cell number. Cells were washed twice with PBS and lysed with RIPA buffer. Samples were resolved on 4–20% precast polyacrylamide gels (BioRad, 4561095). Protein was transferred onto PVDF membranes and blocked with TBST (50 mM Tris, 150 mM NaCl, 0.1% Tween 20) and 5% milk for 1 h at room temperature. Samples were probed overnight at 4 °C in a shaking incubator with the indicated primary antibodies. Soluble APOE was quantified from medium condition by pericytes for 48 h using an APOE ELISA kit (Thermo Fisher Scientific, EHAPOE). Uncropped western blot images are provided in source data.

RNA analysis of iPSC-derived cell lines. Total RNA was isolated using Trizol and zymogen RNA-direct spin column treated with DNase on a column for 30 min before washing and elution. For RT–PCR, 500 ng of total RNA was reverse transcribed into cDNA with iScript (BioRad). Expression was quantified by SsoFast EvaGreen supermix (BioRad). For RNA-seq, extracted total RNA was subject to QC using an Advanced Analytical-fragment Analyzer before library preparation using an Illumina Neoprep stranded RNA-seq library preparation kit. Libraries were pooled for sequencing using Illumina HiSeq2000 or NextSeq500 platforms at the MIT Biomicro Center. Raw fastq data were aligned to human hg19 assembly using STAR 2.4.0 RNA-seq aligner[53]. Mapped RNA-seq reads covering the edited *APOE3/4* site were used to validate data genotypes. Gene raw counts were generated from mapped data using the feature Counts tool[54]. Mapped reads were also processed by Cufflinks2.2 (ref. [55]) with hg19 reference gene annotation to estimate transcript abundances. A gene differential expression test between *APOE3* and *APOE4* groups of each cell type was performed using Cuffdiff module with adjusted q value <0.05 for statistical significance. The geometric method was chosen as the library normalization method for Cuffdiff. Color-coded scatter-plots were used to visualize group FPKM values for DEGs and other genes.

Single-nucleus RNA-seq and human postmortem tissue staining. Human hippocampal single-nuclei transcriptomic data profiled as part of The Religious Orders Study and Rush Memory and Aging Project[56] (www.synapse.org/#!Synapse:syn3219045) were analyzed for computational identification and extraction of pericyte and endothelial single-cell transcriptomes. Putative pericyte and endothelial cells were identified by annotating groups of clustering cells presenting enriched expression of either pericyte or endothelial markers. Identified cells formed disjointed cell groups that did not display enrichment of neuronal, oligodendrocyte, oligodendrocyte progenitors, microglia or astrocyte markers. Cell type annotation was conducted using ACTIONet computational framework (http://compbio.mit.edu/ACTIONet/), considering curated gene marker sets reported by Wang et al.[57]. A total of 614 putative endothelial and 4,523 putative pericyte cells with detected expression of either APOE, NFATC1 or NFATC2 were detected and considered for analysis. Corresponding gene counts are reported in (Supplementary Table 1). Differential expression for APOE and NFAT genes in APOE4 versus noncarrier cells was measured using a two-sided Wilcoxon rank-sum test, considering cells with detected expression for the genes. snRNA-seq of PFC from Mathys et al.[57] was analyzed further to identify putative pericytes and endothelial cells by extracting a cluster of cells specifically enriched with expression of pericyte markers (n = 495 identified cells). Human postmortem tissues were

stained as described by Mathys et al.[40] with the exception that hippocampal sections had been imbedded in paraffin and therefore, xylene deparaffination and rehydration steps preceded the staining protocol.

In vivo administration of cyclosporine A. All experiments were performed according to the Guide for the Care and Use of Laboratory Animals and were approved by the National Institutes of Health and the Committee on Animal Care at the Massachusetts Institute of Technology. 5XFAD mice were obtained from the Jackson Laboratory (34848-JAX) and APOE4KI mice were obtained from Taconic. 5XFAD and APOE4KI mice were crossed for at least eight generations. CsA was prepared 1 mg ml^{-1} in olive oil and injected interperitoneally at a concentration of 10 mg kg^{-1} into 6-month-old female mice daily for 3 weeks. Animals were anesthetized with gaseous isoflurane and transcardially perfused with ice-cold PBS. Brains were dissected out and split sagittally. One hemisphere was frozen and one was post-fixed in 4% paraformaldehyde at 4 °C overnight. The fixed hemisphere was sliced at a thickness of 40 µM using a Leica vibratome. Slices were blocked for 2 h at room temperature and then incubated with primary antibody overnight at 4 °C, subsequently washed five times for 10 min in PBS and incubated with secondary antibody and Hoechst (1:10,000 dilution) for 2 h at room temperature. Slices were then washed five times for 10 min in PBS then mounted for imaging. Researchers performing imaging, quantification and analysis were blinded to the experimental group of each mouse and unblinded only following analysis.

Isolation of mouse primary brain pericytes. Primary brain pericytes were isolated from 6–8-week-old APOE4KO mice as previously described[58]. Primary brain pericytes were subsequently expanded for at least two passages and then treated with 2.5 µM CsA or 5 µM FK506 for 2 weeks. Gene expression was analyzed by qRT–PCR for human APOE and normalized to mouse GAPDH.

Statistics. Statistical analysis was performed using GraphPad Prism 6.0. Correction for multiple comparisons were included when needed. The number of replicates and tests employed are detailed in figure legends.

Reporting Summary. Further information on research design is available in the Nature Research Reporting Summary linked to this article.

Data availability

All requests for raw and analyzed data and materials are promptly reviewed by the Massachusetts Institute of Technology, Technology Licensing Office to verify whether the request is subject to any intellectual property or confidentiality obligations. Patient-related data not included in the paper were generated as part of clinical trials and may be subject to patient confidentiality. Any data and materials that can be shared will be released via a Material Transfer Agreement. All raw and analyzed sequencing data can be found at the NCBI Sequence Read Archive (accession number: GSE125869).

References

53. Dobin, A. et al. STAR: ultrafast universal RNA-seq aligner. *Bioinformatics* **29**, 15–21 (2013).
54. Liao, Y., Smyth, G. K., Bioinformatics, W. S. featureCounts: an efficient general purpose program for assigning sequence reads to genomic features. *Bioinformatics*. **7**, 923–930 (2014).
55. Trapnell, C. et al. Differential gene and transcript expression analysis of RNA-seq experiments with TopHat and Cufflinks. *Nat. Protoc.* **7**, 562–578 (2012).
56. Bennett, D. A. et al. Religious orders study and rush memory and aging project. *J. Alzheimer's Dis.* **64**, S161–S189 (2018).
57. Wang, J. et al. Gene expression distribution deconvolution in single-cell RNA sequencing. *Proc. Natl Acad. Sci. USA* **115**, E6437–E6446 (2018).
58. Boroujerdi, A. et al. Isolation and Culture of Primary Pericytes from Mouse Brain. *Cerebral Angiogenesis*. 383–392 (2014).

Acknowledgements

We thank J. Penny, W.C. Huang, Y.M. Yang and P. Narayan for critically reading the manuscript, J.Z. Young, J. Ray, V. Buggia-Prevot, C. Fernandez, the Neurodegenerative Consortium and all Tsai laboratory members for helpful discussions, A. Marco for expertise and support with microscopy, J. Seo for expertise and guidance with western blotting and Y. Zhou, E. McNamara, P. Curtis and T. Garvey for administrative support. This work was supported by The Neurodegeneration Consortium, the Belfer Family Foundation and the Oskar Fisher Project to L.-H.T., Cure Alzheimer's Fund to L.-H.T. and MK, RF1 AG062377 to L-HT and MK, RF1 AG048056. The National Institutes of Health Common Fund's Library of Integrated Network-based Cellular Signatures program by U54HG008097 to L.-H.T. and J. Jaffe (Broad Institute), P30AG10161, R01AG15819, R01AG17917, U0161356 to D.A.B., UG3NS115064 to L.-H.T. and J.W.B. M.B.V. is supported by the HHMI Hannah Gray Postdoctoral Fellowship. J.W.B. was supported in part by The Glenn Foundation for Medical Research and American Federation for Aging Research Postdoctoral Fellowship during this work.

Author contributions

J.W.B. and L.-H.T. conceived the study. J.W.B., M.B., L.A.A., L.Z., A.F., M.B.V. and J.M.B. performed experiments and analyzed results. H.P.C. performed RNA-seq genomic alignments and DEG analysis. J.D.-V. and H.M. performed and analyzed the snRNA-seq experiments. Y.-T.L. generated isogenic and knockout APOE lines. T.K. generated the iPSC lines used in this study. J.W.B, L.-H.T. and H.P.C. wrote and revised the manuscript.

Competing interests

L.-H. Tsai and J. Blanchard filed a patent application on the iBBB technology (PCT/US2020/014572). The authors declare no other competing interests.

Additional information

Extended data is available for this paper at https://doi.org/10.1038/s41591-020-0886-4.

Supplementary information is available for this paper at https://doi.org/10.1038/s41591-020-0886-4.

Correspondence and requests for materials should be addressed to L.-H.T.

Peer review information Kate Gao was the primary editor on this article, and managed its editorial process and peer review in collaboration with the rest of the editorial team.

Reprints and permissions information is available at www.nature.com/reprints.

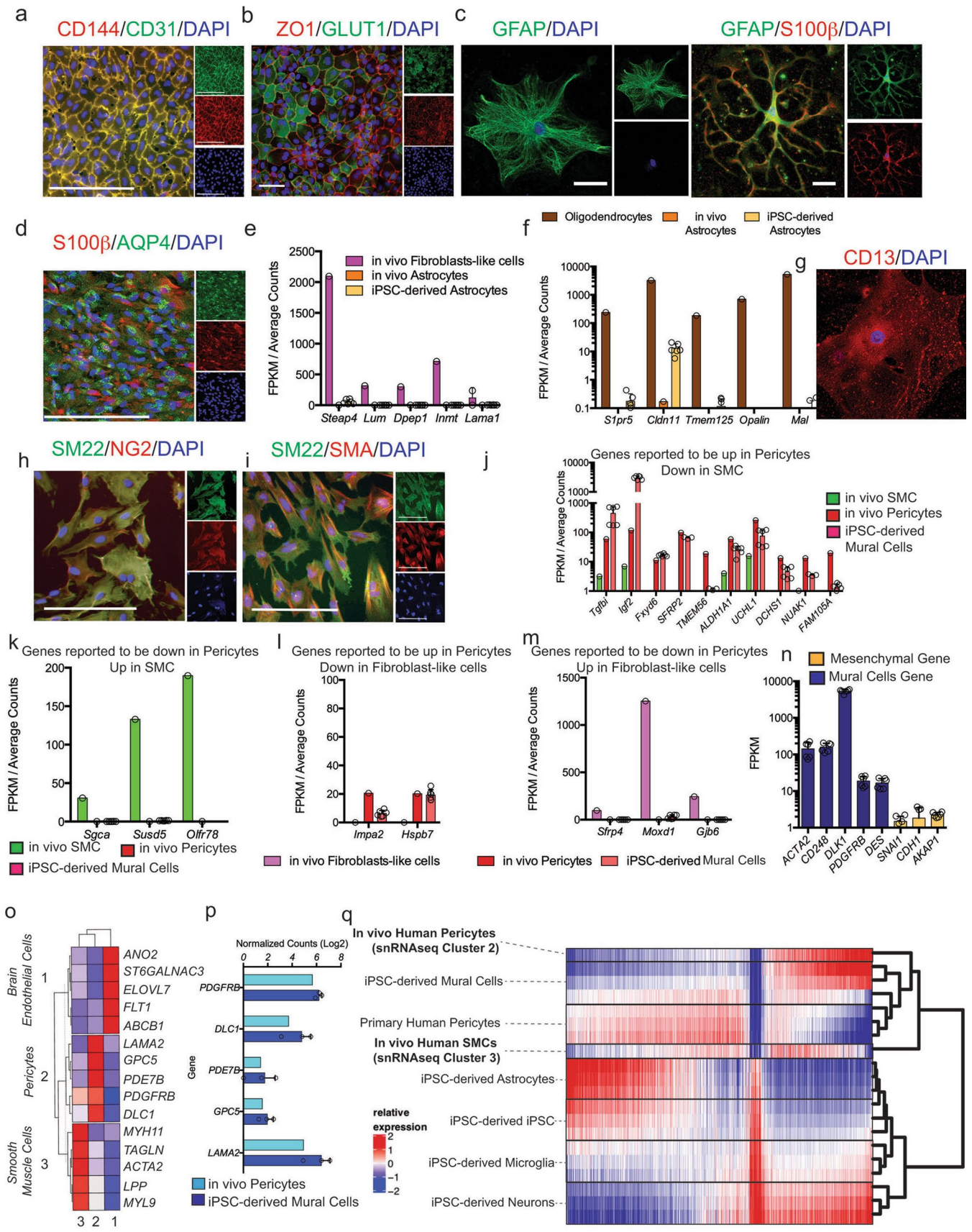

Extended Data Fig. 1 | See next page for caption.

Extended Data Fig. 1 | Characterization of human iPSC-derived cells. a and **b** iPSC-derived brain endothelial cells stained with CD144 (VE-Cadherin), CD31 (PECAM), ZO-1 and GLUT1. These experiments were repeated at least 4 times with similar results. **c** and **d**, iPSC-derived astrocytes stained with GFAP, S100β and AQP4. **e** and **f** Comparative expression analysis of genes in iPSC-derived astrocytes from RNA-sequencing that are reported to be the most differentially upregulated in These experiments were repeated at least 4 times with similar results. **e**, fibroblasts and **f**, oligodendrocytes when compared to astrocytes from In vivo data in Vanlandewijck et al., 2018. Astrocytes are from 6 independent bulk RNA-sequencing **g-i** iPSC-derived mural cells stained with CD13, SM22, NG2, and SMA. These experiments were repeated at least 2 times with similar results. **j**. Comparative expression analysis of the top differentially upregulated genes in pericytes compared to smooth muscle cells (SMCs) from In vivo data in Vanlandewijck et al., 2018. iMCs are from 6 independent bulk RNA-sequencing. Expression is represented as FPKM values from bulk RNA-sequencing. Center values are mean and error bars are SD **k**, Comparative expression analysis of the top differentially upregulated genes in SMCs compared to pericytes from In vivo data in Vanlandewijck et al., 2018. iMCs are from 6 independent bulk RNA-sequencing. Expression is represented as FPKM values from bulk RNA-sequencing Center values are mean and error bars are SD **l**, Expression of the top three differentially upregulated genes in pericytes compared to fibroblasts. **m**, Expression of the top three differentially upregulated genes in fibroblasts compared to pericytes from In vivo data in Vanlandewijck et al., 2018. iMCs are from 6 independent bulk RNA-sequencing. Center values are mean and error bars are SD. **n**, Expression of mural cells and mesenchymal marker genes in iPSC-derived mural cells. For e, f, j, k, l, m, differential gene lists are based on analysis provided shown as average counts compared to FPKM from bulk RNA-sequencing of iPSC-derived astrocytes and mural cells. Center value and error bars are means and SD from RNA prepared from 6 independent wells. **o**, Identification of In vivo Brain Endothelial, Pericyte, and SMC cluster via marker gene expression from single-nucleus RNA-sequencing of the human post-mortem hippocampus from 82 individuals. **p**, iPSC-derived mural cells express markers of in vivo human brain pericytes. Center values and error bars are means and SD from independent RNA prepared from 3 separate wells. **q**, Global hierarchical clustering of transcriptomes (13,338 genes) demonstrates that iPSC-derived mural cells cluster with in vivo human hippocampal pericytes. Clustering was performed by average correlation with simple linkage.

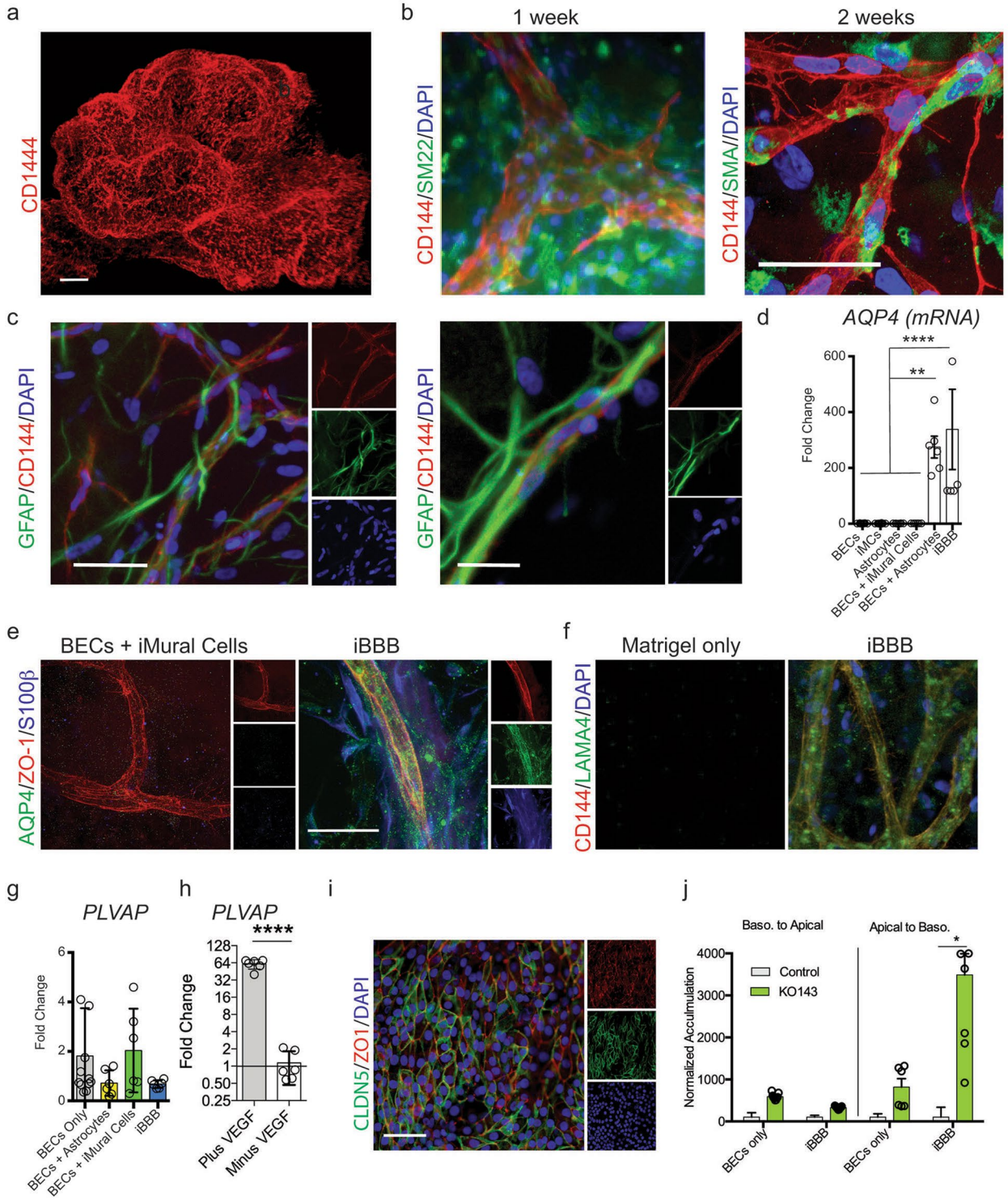

Extended Data Fig. 2 | See next page for caption.

Extended Data Fig. 2 | Characterization of human iBBB. a, Three-dimensional vascular network of endothelial cells stained with CD144 scale bar = 200 μm. **b**, one week after formation iMural cells labeled with SM22 are homogeneously dispersed and rudimentary vessels started forming. After two weeks endothelial vessels formed and iMural cells have homed to perivascular space. **c**, Astrocytes are dispersed throughout iBBB cultures. Experiments in a-c were repeated at least 3 times. **d**, mRNA expression of AQP4 in each cell type alone, pair-wise and combined. One-way ANOVA with Bonferroni's multiple comparison. **, $p = 0.0013$, 0.002, 0.0035, and 0.0076 for BECs, iMCs, Astrocytes, and BECs + iMCs respectively. ****, $p < 0.0001$. Center values and error bars are means and SDs from 6 independent RNA isolations. **e**, iBBB without astrocytes do not stain for AQP4 (green). In iBBBs with astrocytes AQP4 densely stains along endothelial vessels. **f**, Immunostaining for LAMA4 showing that Matrigel does not contain LAMA4 however iBBB cultures remodel basement membrane surrounding endothelial vessels to contain LAMA4. Experiments in e-f were repeated at least 3 times. **g**, PLVAP mRNA expression is upregulated in BECs from iBBB cultures compared to BECs cultured alone. Center values and error bars are mean and SD from RNA harvested from six independent wells. **h**, PLVAP mRNA expression is downregulated in BECs from iBBB upon removal of VEGFA from culture media. Center values and error bars are mean and SD from RNA harvested from six independent wells. Two-sided unpaired student t-test $p < 0.0001$. **i**, iBBB cultured in trans-well format express high levels of BBB marker CLDN5 (green) and ZO1 (red). Experiments in e-f were repeated at least 2 times. **j**, Polarization of ABCG2 was measured by Hoechst transport for both a BECs monolayer and the iBBB from the apical to the basolateral surface and *vice versa*. Samples treated with the ABCG2 specific inhibitor KO143 were normalized to each respective non-inhibitor treated sample. Stars represent significance determined by two-sided multiple student's t-test (FDR = 0.01; $p = 0.0011$) Center values and error bars are mean and SD from 6 independent transwells.

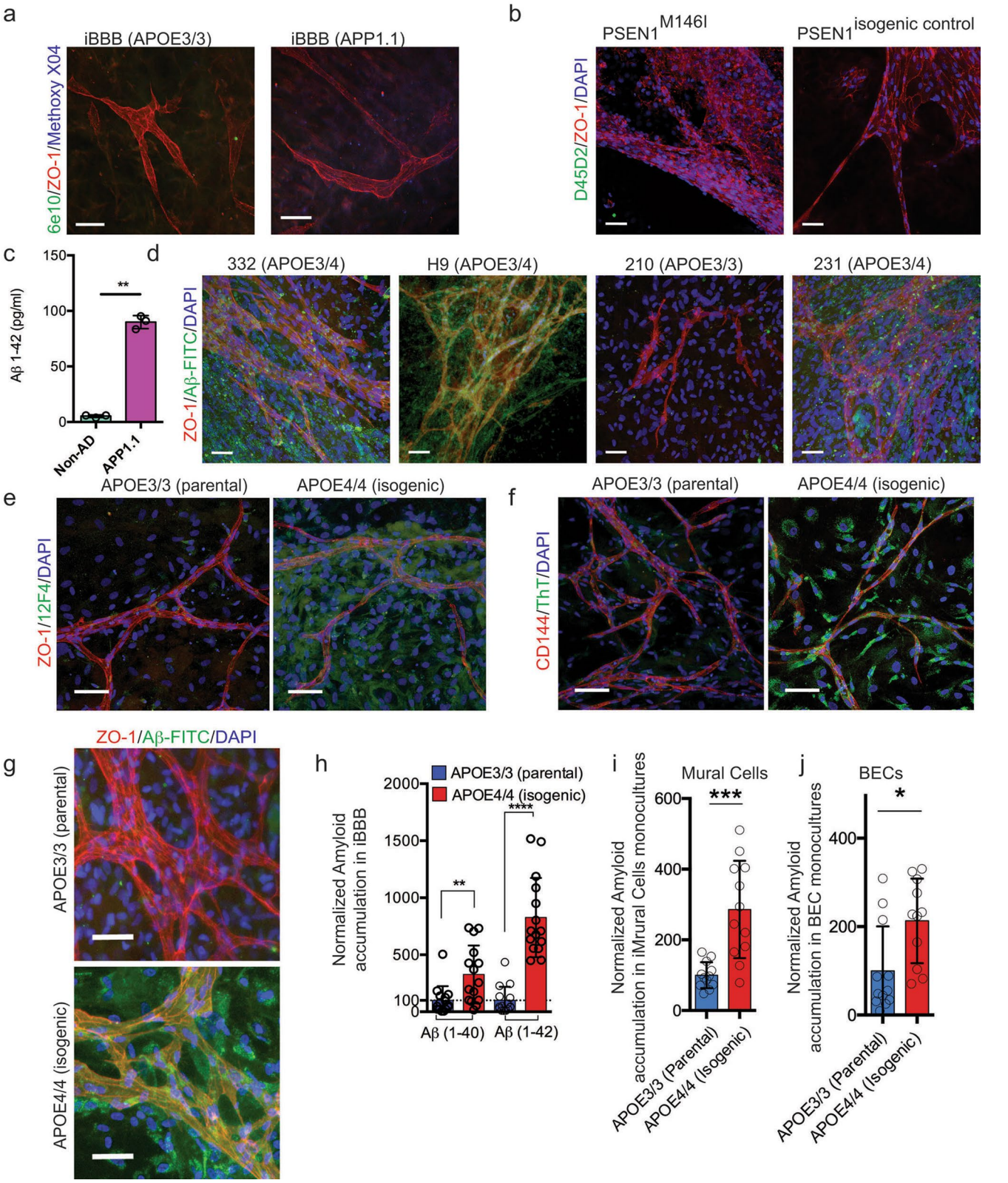

Extended Data Fig. 3 | See next page for caption.

Extended Data Fig. 3 | Validation of the iBBB as a model for CAA. a, iBBBs generated from a familial AD patient iPSC with duplication of the *APP* gene (APP1.1) do not inherently have higher amyloid levels than non-AD controls (AG09173). **b**, iBBBs generated from iPSCs with a familial AD-associated mutation (M146I) in the *PSEN1* gene do not inherently have higher amyloid levels than its non-AD isogenic control. Experiments in a and b were repeated at least 3 times. **c**, Media conditioned by neuronal cells derived from familial AD patient has significantly higher Aβ(1-42). Two-sided Student t-test ($p = 0.0022$) Center values and error bars are mean and SD from 3 independent wells. **d**, Representative images depicting that iBBBs derived from APOE3/4 individuals exhibit high levels of amyloid accumulation relative to iBBBs generated from APOE3/3 individuals. **e** and **f**, Representative images depicting that iBBBs derived from isogenic APOE3/3 and APOE4/4 individuals exhibit high levels of amyloid accumulation assay with anti-amyloid antibody Thioflavin T (f) and 12F4 (e). Experiments in d-f were repeated at least 3 times. **g** and **h**, Representative images and quantification of amyloid accumulation in isogenic iBBBs exposed to 20 nM Aβ-FITC for 1–40 and 1–42 isoforms. The total area positive for amyloid was divided by total nuclei and then normalized to the mean amyloid/nuclei from all E3/3 samples such that the mean of E3/E3 is set to 100% for each isoform. Students t-test, 1–40 $p = 0.0044$; 1–42 $p > 0.00001$. Experiments in were repeated at least 3 times. Center values and error bars are means and SD from 12 independent iBBBs. **i** and **j**, Normalized amyloid accumulation in isogenic iMural cells and BECs mono-culture for each APOE genotype. Two-sided Students t-test, iMural cells, $p = 0.0002$; BECs $p = 0.0118$. Center values and error bars are means and SD from 12 independent wells.

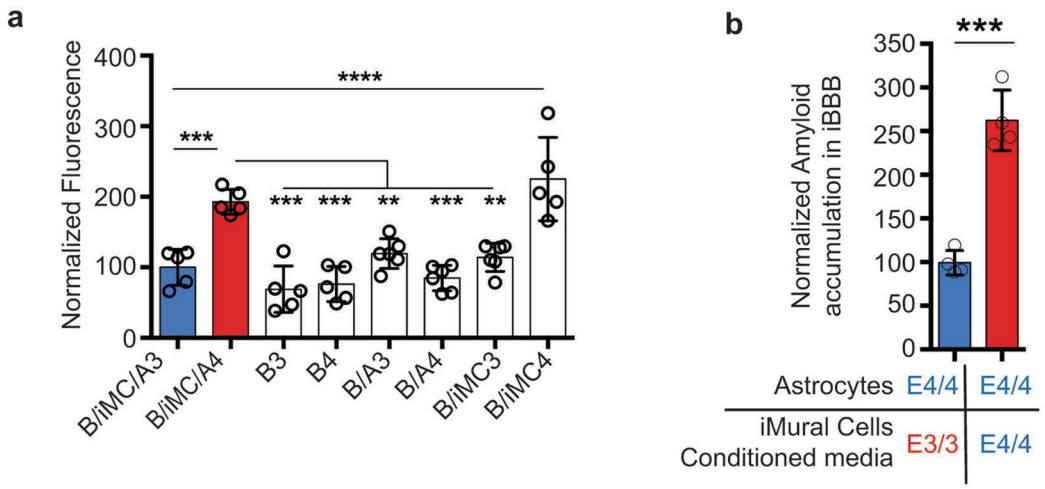

c

Up regulated Biological processes

	ID	Name	pValue	FDR B&H	FDR B&Y	Bonferroni	Genes from Input	Genes in Annotation
1	GO:0006614	SRP-dependent cotranslational protein targeting to membrane	1.16E-59	1.09E-55	1.06E-54	1.09E-55	79	94
2	GO:0006613	cotranslational protein targeting to membrane	5.70E-58	2.66E-54	2.59E-53	5.32E-54	81	101
3	GO:0045047	protein targeting to ER	2.07E-54	6.46E-51	6.28E-50	1.94E-50	79	102
4	GO:0072599	establishment of protein localization to endoplasmic reticulum	1.54E-53	3.61E-50	3.51E-49	1.44E-49	80	106
5	GO:0070972	protein localization to endoplasmic reticulum	1.02E-50	1.91E-47	1.86E-46	9.56E-47	85	125

Down regulated regulated Biological processes

	ID	Name	pValue	FDR B&H	FDR B&Y	Bonferroni	Genes from Input	Genes in Annotation
1	GO:1903047	mitotic cell cycle process	4.27E-28	2.32E-24	2.23E-23	3.55E-24	200	931
2	GO:0000278	mitotic cell cycle	5.59E-28	2.32E-24	2.23E-23	4.65E-24	212	1016
3	GO:0022402	cell cycle process	5.49E-25	1.52E-21	1.46E-20	4.57E-21	255	1385
4	GO:0007049	cell cycle	3.37E-24	7.00E-21	6.72E-20	2.80E-20	302	1766
5	GO:0000280	nuclear division	5.35E-22	8.90E-19	8.55E-18	4.45E-18	137	599

Extended Data Fig. 4 | APOE4 Pericytes Increase CAA pathology in iBBB. a, Quantification of Aβ accumulation in deconstructed iBBBs. B/iMC/A3 and B/iMC/A4 indicate all APOE3/3 and APOE4/4 iBBBs respectively where B = BECs only, B/A = BECs and astrocytes, and B/iMC = BECs and iMural cells. Analysis was performed by One-way ANOVA with Bonferroni's post-hoc analysis ($p < 0.0001$). Center values and error bars are means and SD from 5 independent iBBBs. B/iMCA3 v B/iMCA4, $p = 0.0005$; B/iMCA4 v- B3, $p = 0.0001$; B4, $p = 0.0001$; B/A3, $p = 0.0064$; B/A4, $p = 0.0001$; B/iMC3, $p = 0.0026$; B/iMC/A3 v B/iMC4, $p < 0.0001$. **b**, Exposing APOE4/4 astrocytes to APOE4/4 iMural cell conditioned media significantly increases amyloid accumulation compared APOE3/3 pericyte conditioned media. Unpaired two-sided Student t test, $p = 0.0001$. Center values and error bars are means and SD from 4 iBBBs. **c**, GO analysis from Toppfun (statistics described at https://toppgene.cchmc.org/enrichment.jsp) depicting biological processes associated with up-regulated and down-regulated genes. From RNA extracted from 3 independent wells of iMCs for each genotype.

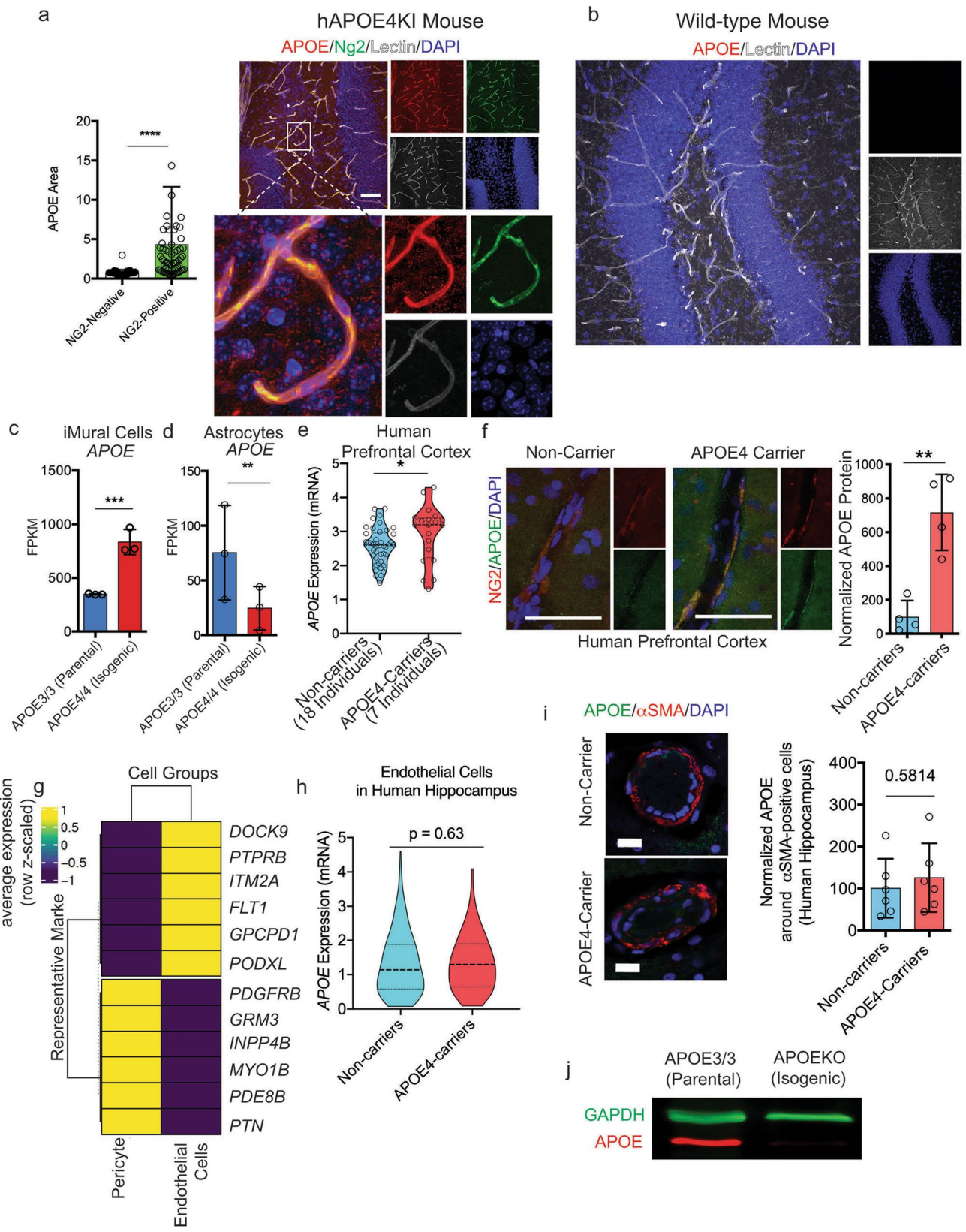

Extended Data Fig. 5 | See next page for caption.

Extended Data Fig. 5 | APOE expression is selectively elevated in APOE4 pericytes. a, Quantification and representative image of APOE protein expression in brain vascular pericytes (NG2-positive cells) and non-pericytes (NG2-negative) cells in APOE4 knock-in mouse. Two-sided Student t test, $p < 0.0001$ Scale bar = 50 um. Center values and error bars are means from 150 APOE-positive cells for each genotype. **b**, anti-APOE antibody (Abcam, ab52607) is specific for human APOE protein and does not react with mouse Apoe protein or other proteins present in wild-type mouse hippocampus as reported by the manufacturer. The staining was repeated using 3 different mice **c** and **d**, Expression of APOE in isogenic iMural cells (c) and astrocyte (d) measured by RNA sequencing each condition represents three biological replicates pericyte, $q = 0.0003$ astrocyte, $q = 0.0006$ statistics performed by Dseq2, Center values and error bars are mean and SD from RNA prepared from 3 independent wells for each genotype. **e** Violin plots depicting *APOE* expression in pericytes/endothelial cells isolated from post-mortem prefrontal cortex of APOE4-carriers ($n = 7$) compared to non-carriers ($n = 18$). Differential expression was measured using a two-tailed Wilcoxon rank sum test, considering cells with detected expression of APOE ($p = 0.0026$). **f**, Images and quantification of APOE protein expression in post-mortem human prefrontal cortex from APOE4 carriers and non-carriers. Unpaired two-tailed t test ($p = 0.023$). Center values and error bars are mean and SD from staining of 4 prefrontal cortex sections from 4 different individuals. **g**, Differential plot of representative maker genes showing that pericytes and endothelial cells isolated from human hippocampus segregated into distinct cellular clusters ($n = 82$ individuals). **h**, Violin plots depicting *APOE* expression in endothelial cells isolated from post-mortem hippocampus APOE4-carriers ($n = 16$) compared to non-carriers ($n = 46$). Differential expression was measured using a two-tailed Wilcoxon rank sum test, considering cells with detected expression of APOE. Center lines are mean and dashed line are SD. **i**, Images and quantification of APOE protein expression α-SMA positive SMC in post-mortem human hippocampus from APOE4 carriers and non-carriers. Unpaired two-tailed t test ($p = 0.5814$). Center values are mean and SD of hippocampal sections from 6 individuals for each genotype. **j**, Western blot of APOE and GAPDH protein in a isogenic iPSC line in which the APOE gene was truncated via CRISPR-editing to yield a line that does not express of APOE protein and therefore is termed APOEKO line. The experiment was repeated at least 3 time with similar results.

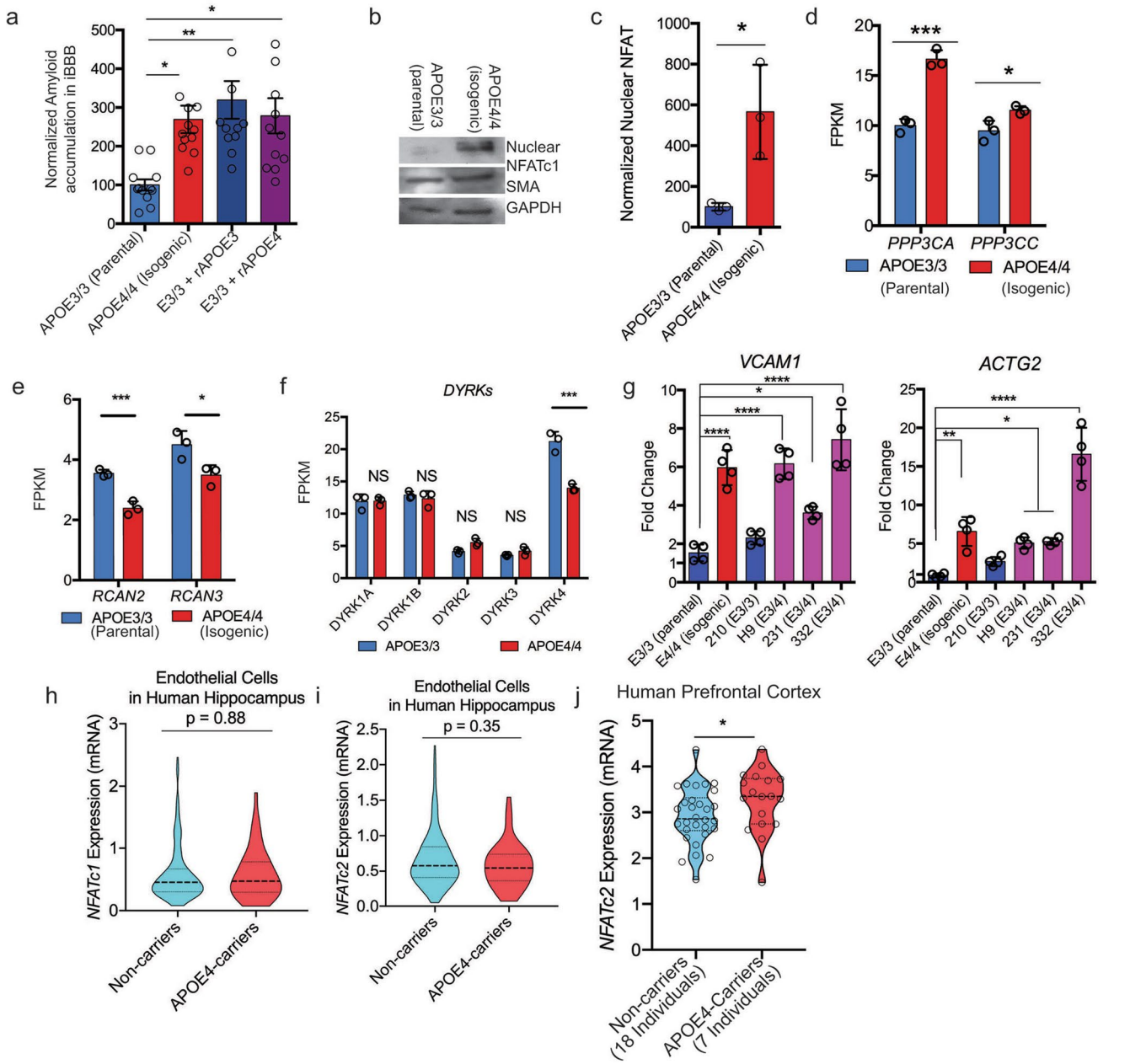

Extended Data Fig. 6 | NFAT/Calcineurin signaling is selectively elevated in APOE4 pericytes. a, Increasing the soluble APOE concentration through the addition of recombinant APOE protein to iBBB culture increases amyloid accumulation. One-way ANOVA with Bonferroni's post-hoc analysis. Center values and error bars are mean and SD from 4 independent iBBBs for each condition. One-way ANOVA with Bonferroni's multiple comparison test. APOE3/3 (Parental) V: APOE4/4 (Isogenic), $p = 0.02$; E3/3 + rAPOE3, $p = 0.0034$; E3/3 + rAPOE4, $p = 0.0144$. **b** and **c**, Representative western blot and quantification depicting nuclear NFATc1 expression in isogenic APOE3 and 4 iMural cells. Unpaired student t test, $p = 0.0254$. Experiment was repeated 3 times with similar results. (c) Center values and error bars are mean and SD from 3 independent lysate preparations for each genotype. **d**, Expression of calcineurin catalytic subunits measured by RNAseq. *PPP3CA* ($q = 0.0003$); *PPP3CC* ($q = 0.0188$). Analysis from DSEQ2. Center values and error bars are mean expression and SD of RNA prepared from 3 independent wells for each genoptype. **e**, Expression of negative *Regulators of Calcineurin* genes (RCANs) measured by RNAseq. *RCAN2* ($q = 0.0003$); *RCAN3* ($q = 0.0123$).). Analysis from DSEQ2. Center values and error bars are mean expression and SD of RNA prepared from 3 independent wells for each genoptype. **f**, Expression of DYRKs kinases known to phosphorylate NFAT measured by RNAseq. *DYRK4* ($q = 0.0003$). Analysis from DSEQ2. Center values and error bars are mean expression and SD of RNA prepared from 3 independent wells for each genoptype. **g**, Expression of predicted NFAT response gene, *VCAM1* and *ACTG2*, in iMural cells. Expression is quantified by qRT-PCR and normalized to the average of E3/3 cells. Significance determined by One-way ANOVA ($p < 0.0001$) with Bonferroni's multiple comparison. For VCAM1 E3/3 (Parental) v- E4/4 (Isogenic), $p < 0.0001$; H9, $p < 0.0001$; 231, $p = 0.0152$; 332, $p < 0.0001$. For ACTG2 E3/3 (Parental) v- E4/4 (Isogenic), $p = 0.0006$; H9, $p = 0.0108$; 231, $p = 0.0076$; 332, $p < 0.0001$. Center values and error bars are mean expression and SD of RNA prepared from 4 independent wells for each cell line. **h** and **i**, Violin plots depicting NFATC1 (h) and NFATC2 (i) expression in pericytes isolated from post-mortem prefrontal cortex of APOE4-carriers ($n = 16$) compared to non-carriers ($n = 46$). Differential expression was measured using a two-tailed Wilcoxon rank sum test, considering cells with detected expression of APOE. Center lines are mean and dashed line are SD. **j** and **k**, Violin plots depicting NFATC2 expression in endothelial cells isolated from post-mortem prefrontal cortex of APOE4-carriers ($n = 7$ compared to non-carriers ($n = 18$). Differential expression was measured using a two-tailed Wilcoxon rank sum test, considering cells with detected expression of APOE ($p = 0.035$). Center lines are mean and dashed line are SD.

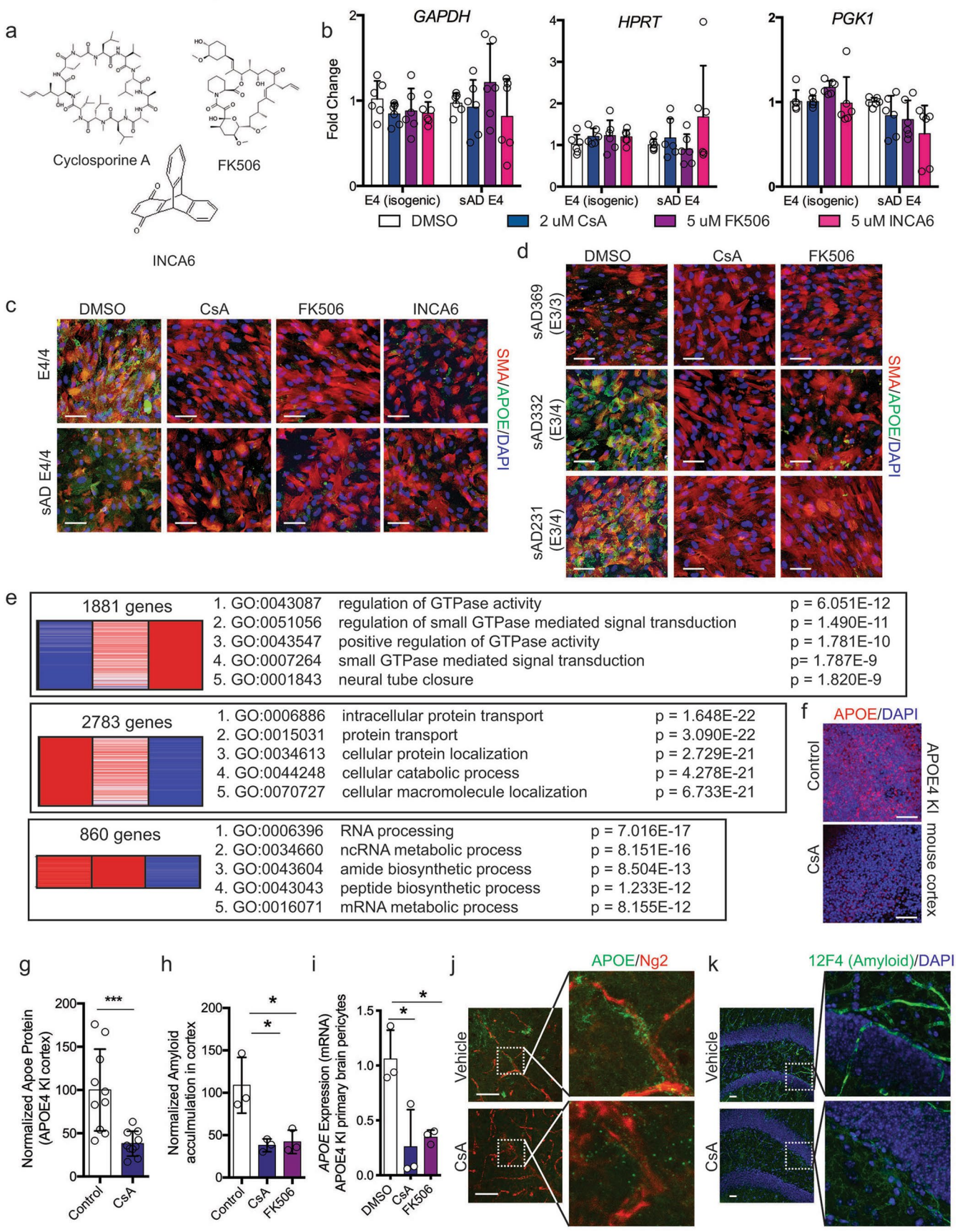

Extended Data Fig. 7 | See next page for caption.

Extended Data Fig. 7 | Inhibiting NFAT/Calcineurin signaling reduces APOE expression and CAA pathology. a, Chemical structures of CsA, FK506, and INCA6 showing highly dissimilar structures. **b**, Expression of PGK1, HPRT, and GAPDH in pericytes after two weeks with DMSO, Cyclosporine A (CsA), FK506 or INCA6. One-way ANOVA ($p < 0.0001$) with Bonferroni's multiple comparison. Center values and error bars are mean expression and SD of RNA prepared from 4 independent wells for each cell line. **c** and **d**, Representative immunofluorescence imaging of APOE protein staining in pericytes after two weeks of treatment with chemicals. Scale bar, 50 μm. Experiments were repeated at least 3 times with similar results. **e** DEGs and associated GO terms for up-regulated and down-regulated genes in E3 and E4 CsA-treated pericyte from RNA-sequencing of RNA prepared from 3 independent wells for each condition. DEGs were determined by DSEQ2 and GO analysis was performed with Toppfun. **f** and **g**, Representative imaging and quantification depicting APOE protein expression in the APOE4KI mouse cortical slices following treatment with cyclosporine A (CsA) for one week. Unpaired, two tailed t test ($p = 0.0009$). Experiments were repeated with similar results using at least 3 slice preparations for each condition. Center values and error bars are mean intensity and SD from 12 independent measurements. **h**, Quantification of amyloid APOE4KI mouse cortical slices treated with either CsA or FK506 for one week and then exposed to 20 nM Ab for 48 hours. One-way ANOVA ($p = 0.0105$) with Bonferroni's multiple comparison. Control v- CsA, $p = 0.0188$; FK506, $p = 0.0245$. Center values and error bars are mean and SD from slices prepared from 3 different mice. **i**, APOE mRNA expression in primary pericytes isolated from brain microvasculature of APOE4 knock-in mice treated with DMSO, Cyclosporine A, or FK506. One-way ANOVA ($p = 0.0139$) with Bonferroni's multiple comparison. For DMSO v- CsA, $p = 0.0221$; FK506, $p = 0.0367$. Center values and error bars are mean and SD from pericytes prepared from 3 different mice. **j**, Representative image of immunostaining for APOE in hippocampal pericytes from APOE4 KI x 5xFAD mice treated with cyclosporine A or vehicle for one week. **k**, Representative images of vascular amyloid in the hippocampus following treatment of 6-month-old APOE4KI x 5XFAD female mice with either vehicle or CsA. Amyloid was detected and quantified with two independent anti-amyloid antibodies (6e10 and 12F4). These experiments were repeated 2 times with similar results.

nature research

Corresponding author(s): Li-Huei Tsai

Last updated by author(s): Jan 21, 2019

Reporting Summary

Nature Research wishes to improve the reproducibility of the work that we publish. This form provides structure for consistency and transparency in reporting. For further information on Nature Research policies, see Authors & Referees and the Editorial Policy Checklist.

Statistics

For all statistical analyses, confirm that the following items are present in the figure legend, table legend, main text, or Methods section.

n/a	Confirmed	
☐	☒	The exact sample size (*n*) for each experimental group/condition, given as a discrete number and unit of measurement
☐	☒	A statement on whether measurements were taken from distinct samples or whether the same sample was measured repeatedly
☐	☒	The statistical test(s) used AND whether they are one- or two-sided *Only common tests should be described solely by name; describe more complex techniques in the Methods section.*
☐	☒	A description of all covariates tested
☐	☒	A description of any assumptions or corrections, such as tests of normality and adjustment for multiple comparisons
☐	☒	A full description of the statistical parameters including central tendency (e.g. means) or other basic estimates (e.g. regression coefficient) AND variation (e.g. standard deviation) or associated estimates of uncertainty (e.g. confidence intervals)
☐	☒	For null hypothesis testing, the test statistic (e.g. *F*, *t*, *r*) with confidence intervals, effect sizes, degrees of freedom and *P* value noted *Give P values as exact values whenever suitable.*
☒	☐	For Bayesian analysis, information on the choice of priors and Markov chain Monte Carlo settings
☐	☒	For hierarchical and complex designs, identification of the appropriate level for tests and full reporting of outcomes
☐	☒	Estimates of effect sizes (e.g. Cohen's *d*, Pearson's *r*), indicating how they were calculated

Our web collection on statistics for biologists contains articles on many of the points above.

Software and code

Policy information about availability of computer code

Data collection	No
Data analysis	For RNAseq analysis, gene raw counts were generated from the mapped data using feature Counts tool (Liao et al., 2014b). The mapped reads were also processed by Cufflinks2.2 (Trapnell et al., 2012) with hg19 reference gene annotation to estimate transcript abundances. Gene differential expression test between APOE3 and APOE4 groups of each cell type was performed using Cuffdiff module and DSEQ2 with adjusted q-value < 0.05 for statistical significance. Geometric method was chosen as the library normalization method for Cuffdiff. Images were analyzed by IMARIS and ImageJ Version 2.0.0

For manuscripts utilizing custom algorithms or software that are central to the research but not yet described in published literature, software must be made available to editors/reviewers. We strongly encourage code deposition in a community repository (e.g. GitHub). See the Nature Research guidelines for submitting code & software for further information.

Data

Policy information about availability of data

All manuscripts must include a data availability statement. This statement should provide the following information, where applicable:

- Accession codes, unique identifiers, or web links for publicly available datasets
- A list of figures that have associated raw data
- A description of any restrictions on data availability

All requests for raw and analyzed data and materials are promptly reviewed by the Massachusettes Institute of Technology, Technology Licensing Office to verify if the request is subject to any intellectual property or confidentiality obligations. Patient-related data not included in the paper were generated as part of clinical trials and may be subject to patient confidentiality. Any data and materials that can be shared will be released via a Material Transfer Agreement. All raw and analyzed sequencing data can be found at the NCBI Sequence Read Archive (accession number: GSE125869).

Field-specific reporting

Please select the one below that is the best fit for your research. If you are not sure, read the appropriate sections before making your selection.

☒ Life sciences ☐ Behavioural & social sciences ☐ Ecological, evolutionary & environmental sciences

For a reference copy of the document with all sections, see nature.com/documents/nr-reporting-summary-flat.pdf

Life sciences study design

All studies must disclose on these points even when the disclosure is negative.

Sample size	No sample-size calculations were performed. Sample size was determined to be adequate based on the magnitude and consistency of differences between groups.
Data exclusions	Data was not excluded
Replication	Findings were confirmed with replicate experiments as noted in the figure legends. iPSC differentiations and iBBBs were quality controlled via immunohistochemistry prior to each experiment. This insured a high-degree of reproducibility. BEC differentiation exhibited batch variability based on expression of VE-Cadherin expression. This was likely due to variability in initial cell plating densities noted to be critical in Qian et al., 2017.
Randomization	Samples and treatments for in vitro studies were randomly assigned. Mice were also randomly assigned to treatment groups with the exception of matching age-ranges for each group.
Blinding	Image analysis was automated and blinded.

Reporting for specific materials, systems and methods

We require information from authors about some types of materials, experimental systems and methods used in many studies. Here, indicate whether each material, system or method listed is relevant to your study. If you are not sure if a list item applies to your research, read the appropriate section before selecting a response.

Materials & experimental systems

n/a	Involved in the study
☐	☒ Antibodies
☐	☒ Eukaryotic cell lines
☒	☐ Palaeontology
☐	☒ Animals and other organisms
☒	☐ Human research participants
☒	☐ Clinical data

Methods

n/a	Involved in the study
☒	☐ ChIP-seq
☒	☐ Flow cytometry
☒	☐ MRI-based neuroimaging

Antibodies

Antibodies used

Antibody/Host species/ Vendor Catalogue /No. Dilution
S-100B /Mouse/ Sigma-Aldrich S2532/ 1:500
ZO-1/ Mouse/ Thermo Fisher MA3-39100/ 1:500
VE-Cadherin/CD144 Goat R&D Systems/ AF938/ 1:500
SM22 Rabbit Abcam/ ab14106/ 1:500
Aquaporin 4/ Rabbit/ Thermo Fisher/ PA5-53234/ 1:500
6E10/ Mouse/ BioLegend/ SIG-39320/ 1:500
CD31/PECAM-1 Sheep R&D Systems/ AF806/ 1:500
GAPDH/ Mouse/ Santa Cruz/ Sc-32233/ 1:500
APOE/ Rabbit/ Abcam/ EP1374Y/ 1:500
SMA/ Mouse/ R&D Systems/ MAB1420/ 1:500
GLUT-1/ Rabbit/ abcam/ ab15309/ 1:500
CLDN5/ Mouse/ Thermo Fisher/ 352588/ 1:500
GFAP/ Rabbit/ Millipore Sigma/ AB5804/ 1:500
NFATc1/ Mouse/ Thermo Fisher/ MA3024/ 1:50
Hoechst/ 33342/ Thermo Fisher/ H3570/ 1:2000
NG2/ Mouse/ BDBioscience/ 554275/ 1:2000
D54D2/ Rabbit/ Cell Signaling /8243S/ 1:500
12F4/ Mouse/ BioLegend/ 805501/ 1:500
Thioflavin T/ Sigma-Aldrich/ T3516/ 10 uM
CD13/ Rabbit/ Abcam/ EPR4058/ 1:100

Secondary Antibody
Donkey anti-mouse Alexa 488 Thermo Fisher A-21202 1:1000
Donkey anti-mouse Alexa 555 Thermo Fisher A-31570 1:1000
Donkey anti-goat Alexa Alexa 555 Thermo Fisher A-21432 1:1000
Donkey anti-Rabbit Alexa 488 Thermo Fisher A-21206 1:1000

Validation

Most antibodies were selected from published literature. Where possible they were validated and optimized using human primary cells.

Eukaryotic cell lines

Policy information about cell lines

Cell line source(s)	Human iPSC cell lines used in this study were generated by the Picower Institute for Learning and Memory iPSC core.
Authentication	IPSC lines are confirmed by marker staining, RNAseq, and karyotyping.
Mycoplasma contamination	Lines are routinely tested and found negative for mycoplasma
Commonly misidentified lines (See ICLAC register)	No misidentified cell lines were used

Animals and other organisms

Policy information about studies involving animals; ARRIVE guidelines recommended for reporting animal research

Laboratory animals	Laboratory mice were used for this study including APOE4 targeted replacement mice from Taconic B6.129P2-(Apoetm3(APOE*4)Mae). APOE4 mice were also crossed to 5xFAD (Jackson Laboratory; 34848-JAX) for drug application studies.
Wild animals	No wild animals were used in this study.
Field-collected samples	No field-collected samples were used in this study.
Ethics oversight	All experiments were performed according to the Guide for the Care and Use of Laboratory Animals and were approved by the National Institute of Health and the Committee on Animal Care at Massachusetts Institute of Technology.

Note that full information on the approval of the study protocol must also be provided in the manuscript.